Importin α7 deficiency causes infertility in male mice by disrupting spermatogenesis

Na Liu[1], Fatimunnisa Qadri[1], Hauke Busch[2], Stefanie Huegel[1,3], Gabin Sihn[1], Ilya Chuykin[1,4], Enno Hartmann[3], Michael Bader[1,3] and Franziska Rother[1,3]

[1] Max Delbrück Center for Molecular Medicine, Berlin, Germany. [2] Medical Systems Biology Division, Lübeck Institute of Experimental Dermatology and Institute for Cardiogenetics, University of Lübeck, Lübeck, Germany. [3] Institute for Biology, Center for Structural and Cellular Biology in Medicine, University of Lübeck, Lübeck, Germany. [4] Department of Cell Developmental and Regenerative Biology, Icahn School of Medicine at Mount Sinai, New York, NY, USA

Corresponding author: Franziska Rother (franziska.rother@mdc-berlin.de)

Keywords: importin, karyopherin, spermatogenesis, male fertility, testis

Summary statement

Using two different mouse models, we delineate the morphological and functional impact of importin α7 on spermatogenesis and Sertoli cell function and show that this protein is crucial for fertility in male mice.

Abstract

Spermatogenesis is driven by an ordered series of events, which rely on trafficking of specific proteins between nucleus and cytoplasm. The importin α family of proteins mediates movement of specific cargo proteins when bound to importin β. Importin α genes have distinct expression patterns in mouse testis, implying they may have unique roles during mammalian spermatogenesis. Here we use a loss-of-function approach to specifically determine the role of importin α7 in spermatogenesis and male fertility. We show that ablation of importin α7 in male mice leads to infertility and has multiple cumulative effects on both germ cells and Sertoli cells. Importin α7-deficient mice exhibit an impaired Sertoli cell function, including loss of Sertoli cells and a compromised nuclear localization of the androgen receptor. Furthermore, our data demonstrate devastating defects in spermiogenesis including incomplete sperm maturation and massive loss of sperms that are accompanied by

disturbed histone-protamine-exchange, differential localization of the transcriptional regulator Brwd1 and altered expression of Rfx2 target genes. Our work uncovers the essential role of importin α7 in spermatogenesis and hence in male fertility.

Introduction

The best characterized mechanism of nuclear import consists of importin α and importin β. Importin α proteins are comprised of three main structural domains: a N-terminal region which is the importin β binding (IBB) domain; a central domain containing Armadillo motifs; and a weakly conserved C-terminal region. The central domain of importin α binds Nuclear Localization Signals that are present in the target cargo proteins. Upon cargo binding, importin α binds to importin β via its IBB domain forming a trimeric transport complex, which is translocated into the nucleus via importin β interactions with nucleoporins lining the nuclear pore complex (Macara, 2001; Miyamoto et al., 2012). To date, three importin α subtypes have been identified in *C. elegans* and *D. melanogaster*, while up to seven importin α isoforms have been found in mammals (Kohler et al., 1997; Tejomurtula et al., 2009; Tsuji et al., 1997).

Male reproductive function relies on normal spermatogenesis within the testis seminiferous epithelium. During spermatogenesis, spermatogonia undergo mitosis and differentiate into primary spermatocytes, which process through preleptotene, leptotene, zygotene, pachytene, and diplotene stages of meiosis I to generate secondary spermatocytes. Subsequently, secondary spermatocytes enter the second meiotic division resulting in round spermatids. The haploid round spermatids undergo dramatic morphological changes, and finally differentiate into mature spermatozoa (Russell, 1990).

Sertoli cells are supporting somatic cells essential for the development of male germ cells. It has been shown that number and function of Sertoli cells determine testicular size, germ cell numbers and spermatozoa output (Orth et al., 1988). Sertoli cell functions include providing structural support and nutrition to developing germ cells, coordination of differentiation among several cohorts of germ cells, secretion of seminiferous fluid, phagocytosis of degenerating germ cells and release of spermatids at spermiation (Bellve and Zheng, 1989; Chihara et al., 2013; Clermont, 1993; Russell and Griswold, 1993).

A key feature of Sertoli cell structural support for developing germ cells is the blood-testis barrier (BTB) that resides in tight junctions (TJ) located between adjacent Sertoli cells (Johnson et al., 2008). At the beginning of meiosis, preleptotene spermatocytes ʻpass through’ the BTB. Once the BTB reformed behind them, the germ cells no longer have access to serum

factors and become totally dependent upon Sertoli cells to supply nutrients and growth factors (Walker, 2010). This structural arrangement creates an immunologic barrier by isolating advanced germ cells from the immune system so that their antigens do not stimulate autoimmunity (Johnson et al., 2008; Orth et al., 1988).

The successful completion of spermatogenesis is dependent on successive division and differentiation steps, which require multiple changes in gene expression, coordinated by transcription and other factors expressed within the testis (Eddy and O'Brien, 1998; Hermo et al., 2010). The access of these factors to the nucleus is tightly regulated for these proteins, and it has been postulated that germ cell differentiation is controlled by nucleocytoplasmic transport events (Major et al., 2011). In fact, the mRNAs of different importin α isoforms and of importin β are all expressed in germ cells and Sertoli cells (Major et al., 2011; Shima et al., 2004), raising the possibility that the importin α/β mediated nuclear import pathway is involved in the regulation of spermatogenesis and Sertoli cell function. With respect to protein expression in murine testis, it is currently known that importin α3 (Kpna4) localizes to nuclei of Sertoli cells, pachytene spermatocytes, and round spermatids step 7-8, while importin α4 (Kpna3) is expressed in the cytoplasm of Sertoli cells, mitotic and meiotic spermatocytes as well as round spermatids (Hogarth et al., 2007). Furthermore, our own unpublished data revealed a very distinct expression of importin α1 (Kpna2) in meiotic germ cells of mouse testis. The protein expression of importin α7 in the murine testis has not been evaluated so far and a specific role of a single importin α isoform in spermatogenesis and male reproduction has not been determined.

We have previously shown that in importin α7-deficient mothers, embryonic development stops at the two-cell stage due to a severely disturbed zygotic genome activation, therefore importin α7 is essential for early embryonic development in mice (Rother et al., 2011). In this report, we show that ablation of *Kpna6*, the gene encoding for importin α7, results in a critical defect in spermatogenesis in mice. We demonstrate that importin α7 protein is expressed in the nuclei of round spermatids, elongating spermatids and Sertoli cells. Consistent with this pattern, importin α7 deficiency results in multiple defects in both germ cells and Sertoli cells culminating in oligozoospermia. Our results demonstrate an essential role for importin α7 in male fertility by regulating spermatogenesis and Sertoli cell function.

Results

Importin α7 is essential for male fertility

We generated two mouse lines with targeted disruption of importin α7. In importin $\alpha7^{\Delta IBB/\Delta IBB}$ mice ($\alpha7^{\Delta IBB/\Delta IBB}$), due to unexpected alternative splicing, a shortened mRNA is generated, containing a cryptic translational start site which leads to synthesis of a truncated protein lacking the importin ß binding domain. In importin $\alpha7^{-/-}$ ($\alpha7^{-/-}$), a gene trap cassette in intron1 of *Kpna6* results in a complete loss of the protein (Fig. 1A). Female mice of both lines are infertile (Rother et al., 2011).

Interestingly, male $\alpha7^{-/-}$ mice are fertile, while $\alpha7^{\Delta IBB/\Delta IBB}$ males were found to be sterile, although they were sexually active and produced vaginal plugs in female partners (data not shown). We observed that, although importin α7 protein is missing in all other organs of $\alpha7^{-/-}$ males (Rother et al., 2011), full-length importin α7 protein is still expressed in the testis, whereas it is completely absent from $\alpha7^{\Delta IBB/\Delta IBB}$ testes (Fig. 1B). The reason for the exclusive expression in the testis of $\alpha7^{-/-}$ males is that an alternative promoter and exon1 (exon1A) are used which are located downstream of the gene trap cassette (Fig. 1A-C, confirmed by sequencing; identical to BY353738.1). This leads to synthesis of a full-length and fully functional importin α7 protein (as the regular translational start site is located in exon2). On the contrary, only a truncated non-functional importin α7 is existent in the $\alpha7^{\Delta IBB/\Delta IBB}$ testes (Fig. 1B), which leads to male infertility, suggesting that importin α7 is essential for male fertility.

Disruption of importin α7 gene causes growth retardation, reduced testis size and severe oligozoospermia

The $\alpha7^{\Delta IBB/\Delta IBB}$ and $\alpha7^{-/-}$ mice were born at a lower frequency ($\alpha7^{\Delta IBB/\Delta IBB}$: 18.8%, n=739; $p<0.0001$; $\alpha7^{-/-}$: 16%, n=214, $p=0.0015$) than predicted by Mendelian laws. With regards to growth and development, the heterozygous males are indistinguishable from wildtype (WT) males (data not shown). However, $\alpha7^{\Delta IBB/\Delta IBB}$ pups displayed severe growth retardation in the postnatal phase, and this growth defect persisted until adult life (Fig. 1D). Male $\alpha7^{-/-}$ mice also displayed a significant growth retardation, albeit the effect in young mice was not so strong. At the age of 16 weeks, males of both mutant lines displayed the same reduction in body weight compared to WT males (Fig. 1D). Testes of adult $\alpha7^{\Delta IBB/\Delta IBB}$ mice exhibited a pronounced reduction both in size and weight (Fig. S1A, B) and the testicular weight to body weight ratio was reduced by 40% at the age of 8-10 weeks compared to WT and $\alpha7^{-/-}$ mice,

which displayed a normal relative testis weight and size (Fig. 1E). Plasma testosterone levels were unchanged (data not shown).

Histological analyses revealed that spermatogenesis was drastically altered in importin $\alpha7^{\Delta IBB/\Delta IBB}$, while no major changes were detected in $\alpha7^{-/-}$ compared to WT testes (Fig. 2A). Seminiferous tubules in the $\alpha7^{\Delta IBB/\Delta IBB}$ testes were smaller in diameter than those in both other groups (Fig. 2A and C). The germ cell number was reduced, and the tubular epithelium was disorganized. Moreover, mature spermatozoa were rarely found in the lumen of $\alpha7^{\Delta IBB/\Delta IBB}$ seminiferous tubules, while multinucleated spermatid giant cells were frequently observed (Fig. 2A). There were very few spermatozoa in the caput of $\alpha7^{\Delta IBB/\Delta IBB}$ epididymides, and spermatozoa were hardly detectable in the caudal epididymides by H&E staining (Fig. 2B). Additionally, sloughed germ cells, and germ cell debris were commonly observed in the epididymal lumen of $\alpha7^{\Delta IBB/\Delta IBB}$ males (Fig. 2B). The total cauda epididymal sperm number in $\alpha7^{\Delta IBB/\Delta IBB}$ was only 1.4% of those of WT males (Fig. 2D), moreover, almost all of the residual sperms found in the $\alpha7^{\Delta IBB/\Delta IBB}$ epididymides displayed abnormal heads in contrast to $\alpha7^{-/-}$ and WT sperms (Fig. 2E). Surprisingly, also $\alpha7^{-/-}$ sperm count was significantly reduced, suggesting a partially reduced fertility in these mice (Fig. 2D). In both lines the epididymal sperm count of heterozygous mice was normal (Fig. S1C).

Importin α7 expression pattern in mouse testis

To assess the cell type-specific expression of importin α7 in the testis, we performed immunohistochemistry in WT mice using an antibody which detects the C-terminus of importin α7 (Fig. 3). No importin α7 could be detected in spermatogonia and meiotic spermatocytes. Early round spermatids showed very low levels of expression which increased throughout their development (steps1-8), reaching its highest expression in step9 elongating spermatids (stage IX), where importin α7 displayed a high nuclear and low cytoplasmic expression. With the onset of nuclear elongation, localization of importin α7 shifted to the cytoplasm, and was no longer detectable after the residual bodies were removed in step16 sperms (stage VII-VIII). Importin α7 was highly expressed in the nuclei of Sertoli cells in all stages of the seminiferous epithelium (Fig. 3). The massive increase of importin α7 expression in step9 elongating spermatids, and the high expression level in the nuclei of Sertoli cells suggest an important role of importin α7 in these cells.

As the antibody against the C-terminus of importin α7 detects the full length and the truncated form of the protein, it showed a regular staining in $\alpha7^{\Delta IBB/\Delta IBB}$ testes. Interestingly, testis sections of $\alpha7^{-/-}$ mice revealed that the protein expression is rescued in germ cells, but not in Sertoli cells in this mouse line (Fig. 4A). Spatial and temporal expression of importin α7 in $\alpha7^{-/-}$ germ cells was similar to WT (Fig. 4A, data not shown).

To verify these results, we generated an antibody against the N-terminus of importin α7 that could discriminate between the full-length and the truncated ΔIBB-protein in which the N-terminus is missing (Fig. 1A, B). Staining of testis sections of WT mice showed a robust signal in round and elongating spermatids as well as Sertoli cells. In contrast, no signals could be detected in $\alpha7^{\Delta IBB/\Delta IBB}$ testis sections, confirming the truncation of importin α7 in these mice. In $\alpha7^{-/-}$ testes, the rescued expression in developing spermatids could be verified, while no expression was found in Sertoli cells (Fig. 4B). The missing expression of importin α7 in Sertoli cells could thus account for the reduced sperm cell number observed in $\alpha7^{-/-}$ mice, however, only $\alpha7^{\Delta IBB/\Delta IBB}$ mice are infertile, suggesting, that the expression of the protein in germ cells is indispensable for normal sperm development and fertility.

Thus, $\alpha7^{-/-}$ mice express a mild Sertoli cell-related phenotype, while $\alpha7^{\Delta IBB/\Delta IBB}$ mice express a mixed phenotype consisting of Sertoli cell- and germ cell-related defects. While the infertile $\alpha7^{\Delta IBB/\Delta IBB}$ mice express only truncated importin α7 protein in Sertoli cells and in developing sperms, heterozygous importin $\alpha7^{\Delta IBB/+}$ mice express full-length plus truncated protein, however, sperm count in these mice turned out to be completely normal (Fig. S1C), excluding a dominant negative effect of the truncated protein on sperm count. Moreover, a dominant negative effect on growth defects could as well be excluded (Fig. S1D). To discriminate between Sertoli cell- and sperm cell-related phenotypes, we compared mice of both lines ($\alpha7^{\Delta IBB/\Delta IBB}$ mice vs. $\alpha7^{-/-}$ mice). We rescued the germ cell phenotype without rescueing the Sertoli cell phenotype in $\alpha7^{\Delta IBB/\Delta IBB}$ mice by crossing $\alpha7^{\Delta IBB/\Delta IBB}$ and $\alpha7^{-/-}$ mice. The resulting compound heterozygous $\alpha7^{\Delta IBB/-}$ mice express only the truncated importin α7 in Sertoli cells and truncated plus full-length importin α7 in developing sperms (Fig. S1E, F). Epididymal sperm count revealed a significant increase of sperm number in importin $\alpha7^{\Delta IBB/-}$ mice compared to $\alpha7^{\Delta IBB/\Delta IBB}$ mice (Fig. S1C), suggesting that, indeed, full-length importin α7 in developing sperms can partially rescue the oligozoospermia. Moreover, the sperm count in $\alpha7^{\Delta IBB/-}$ was markedly lower than in WT and comparable to $\alpha7^{-/-}$ mice, confirming that the absence of full-length importin α7 in Sertoli cells is the reason for the partial reduction in sperm count. Thus, we can conclude that importin α7 expression in spermatocytes and round spermatids is essential for normal sperm development and fertility.

Importin α7 deficiency leads to defects in Sertoli cells

Since importin α7 was intensively expressed in the nuclei of WT Sertoli cells, the protein may be essential for the function of these cells. We observed a reduced number of Sertoli cells in testes of adult $\alpha7^{\Delta IBB/\Delta IBB}$ mice and $\alpha7^{-/-}$ mice, suggesting that importin α7 perturbation caused a loss of Sertoli cells (Fig. 5A). Moreover, in both mutant lines Sertoli cells were frequently observed being detached in the middle of seminiferous tubules (Fig. 5B). Interestingly, in young prepubertal mice, no differences in Sertoli cell numbers were detected (Fig. 5A), concluding that the proliferation phase of Sertoli cells was not affected.

The androgen receptor (AR), which is highly expressed in Sertoli cells, plays an important role in spermatogenesis. We observed a pronounced reduction of AR in Sertoli cell nuclei of both mutant lines (Fig. 5C). To test, whether expression of AR-related or Sertoli cell-specific transcripts is affected in importin α7-deficient mice, we analyzed expression levels of AR-regulated genes such as *Rhox5, Pem, Wt1, Clusterin, Gata1, Cldn3, and Cldn11*. No significant differences in mRNA levels were detected for most of these genes. Only *Cldn3* expression was markedly downregulated in $\alpha7^{\Delta IBB/\Delta IBB}$, but not in $\alpha7^{-/-}$ testes (Fig. 5D). To confirm these results, immunostaining of testis sections for CLDN3 was performed, revealing the specific localization in basal TJ of late stage VIII tubules in both mutant mouse lines (Fig. S3A). TJ are a major component of the BTB located between adjacent Sertoli cells. To further analyze possible defects in TJ formation of Sertoli cells, we performed immunostaining for ZO-1, a specific TJ protein, in testis sections. No differences were found in its expression and localization in basal TJ and apical ectoplasmic specializations of stage IV-VI tubules (Fig. S3B). We evaluated the functional integrity of the BTB by incubating testicular protein extracts from WT mice with sera taken from WT, $\alpha7^{\Delta IBB/\Delta IBB}$ or $\alpha7^{-/-}$ mice at 8, 16 and 20 weeks of age. A Western blot analysis revealed in some cases differences in the protein band pattern with additional bands appearing in $\alpha7^{\Delta IBB/\Delta IBB}$ and $\alpha7^{-/-}$ mice sera. Thus, the immunological barrier is leaky and therefore antibodies against testicular antigens are occasionally present in both mutant lines (Fig. S3C). However, a subsequent analysis of the presence of immunoglobulins within testicular tissue in mice of different ages revealed no differences (Fig. S3D). Moreover, by injection of biotin into the testis we could not find a compromised BTB in $\alpha7^{\Delta IBB/\Delta IBB}$ and $\alpha7^{-/-}$ mice (Fig. S3E). These data suggest that the BTB is slightly but not severely impaired.

Further analysis of Sertoli cell cytoskeletal proteins revealed an abnormal localization of the intermediate filament vimentin in Sertoli cells of $\alpha7^{\Delta IBB/\Delta IBB}$ and $\alpha7^{-/-}$ mice. Vimentin-based filaments no longer stretched across the Sertoli cell cytosol but retracted and were wrapped around the cell nuclei (Fig. 6A). In contrast, beta-III tubulin organization was not perturbed in Sertoli cells of $\alpha7^{\Delta IBB/\Delta IBB}$ and $\alpha7^{-/-}$ mice (data not shown), suggesting that there is no general effect on Sertoli cell morphology but rather a specific change in vimentin distribution.

The compromised Sertoli cells lead to defects in sperm orientation in both $\alpha7^{\Delta IBB/\Delta IBB}$ and $\alpha7^{-/-}$ mice. (Fig. 6B). Interestingly, sperm transport through the seminiferous epithelium, which is also dependent on Sertoli cells, was severely disturbed in $\alpha7^{\Delta IBB/\Delta IBB}$ mice, but was found to be unaffected in $\alpha7^{-/-}$ mice (Fig. 6C). In WT testis, only one generation of spermatids was found during the transition from round into elongating spermatids. However, two generations of spermatids were often observed in stages IX-XII in $\alpha7^{\Delta IBB/\Delta IBB}$ mice (Fig. 6D). The additionally found spermatids were more mature with condensed nuclei, implicating that they were not released properly. Although correct spermiation is dependent on Sertoli cells, we could not detect residual sperms in stage IX-XII tubules of $\alpha7^{-/-}$ testes, showing that spermatid persistence is not caused by Sertoli cell defects only. Thus, we conclude that absence of importin α7 leads to disturbed sperm organization in both mutant mouse lines, with more severe appearance in importin $\alpha7^{-/-}$ testes.

Importin α7 deficiency-related loss of spermatocytes starts with leptotene/zygotene transition

To elucidate the start of germ cell loss in importin α7-deficient testes, we quantitatively evaluated developmental steps of spermatogenesis. No differences were detected in germ cells labelled with the pluripotency marker Sall4, excluding a severe loss of spermatogonia (Fig. 7A). We observed that the number of BrdU-labelled preleptotene spermatocytes per tubule in $\alpha7^{\Delta IBB/\Delta IBB}$ were slightly decreased compared to $\alpha7^{-/-}$ and WT mice (Fig. 7A). We next tested for γH2AX, a phosphorylated form of histone 2AX, that exhibits an intense diffuse staining pattern in spermatocytes at the leptotene/zygotene transition in stages X-XI, and exclusively localizes to the sex chromosomes within pachytene spermatocytes (Blanco-Rodriguez, 2009; Celeste et al., 2002; Peters et al., 1997). In $\alpha7^{\Delta IBB/\Delta IBB}$ and $\alpha7^{-/-}$ testes, the numbers of leptotene/zygotene spermatocytes in stages X-XI decreased markedly compared to WT controls while we did not observe differences in the stage-specific appearance of γH2AX-positive chromatin (Fig. 7A, B). Interestingly, we detected a further decrease in the number of stage I-VIII pachytene spermatocytes in $\alpha7^{\Delta IBB/\Delta IBB}$ but not $\alpha7^{-/-}$ testes showing that

$\alpha7^{\Delta IBB/\Delta IBB}$ were more affected than $\alpha7^{-/-}$ testes (Fig. 7A). The ratios of pachytene to leptotene spermatocytes were similar in WT and importin $\alpha7^{-/-}$, while it was markedly reduced in $\alpha7^{\Delta IBB/\Delta IBB}$ testes (wt: 0.94; $\alpha7^{\Delta IBB/\Delta IBB}$: 0.77, $\alpha7^{-/-}$: 1.00), suggesting that development of pachytene spermatocytes is dependent on importin α7. The reduced numbers of step1-8 round spermatids in $\alpha7^{\Delta IBB/\Delta IBB}$ and $\alpha7^{-/-}$ testes were comparable with numbers of pachytene spermatocytes, while the ratios of round spermatids to pachytene spermatocytes were similar between all three groups (Fig. 7A). These observations suggest that deficiency of importin α7 leads to a reduction in leptotene/zygotene spermatocytes, and to a further decrease in pachytene spermatocytes, but surviving spermatocytes can differentiate into round spermatids. The loss of pachytene spermatocytes was accompanied by a higher number of TUNEL-positive cells in importin $\alpha7^{\Delta IBB/\Delta IBB}$ testes (Fig. 7A).

Onset of spermatogenesis is delayed in $\alpha7^{\Delta IBB/\Delta IBB}$ and $\alpha7^{-/-}$ mice

By H&E staining of testes from 6 weeks old mice we discovered a retardation in testis development in $\alpha7^{\Delta IBB/\Delta IBB}$ mice: while WT and $\alpha7^{-/-}$ mice showed a regular histology with seminiferous tubules at various stages, in $\alpha7^{\Delta IBB/\Delta IBB}$ mice, all tubules displayed uniformly the same developmental stage and no round spermatids or later stages could be detected, indicating that the first meiotic wave had not been completed (Fig. 8A). Analysis of meiotic spermatocytes by γH2AX-labelling showed a typical pattern with a short wave of positive nuclei in stage VIII tubules (preleptotene spermotocytes) and a second wave starting in leptotene which peaked in leptotene/zygotene and decreased into small foci in zygotene before γH2AX labelled the sex chromosomes in early pachytene spermatocytes (Blanco-Rodriguez, 2009; Hamer et al., 2003). Analysis of day 21 testes by γH2AX labelling revealed a high number of leptotene/zygotene spermatocytes in $\alpha7^{\Delta IBB/\Delta IBB}$ mice, while in WT testes most of the spermatocytes had already reached pachytene stage and round spermatids started to be present (Fig. 8B, C). Interestingly, $\alpha7^{-/-}$ testes also displayed a higher amount of strongly γH2AX-positive leptotene/zygotene spermatocytes and only few round spermatids were visible (Fig. 8B, C). Together, these data show that, compared with WT mice, the onset of the first wave of spermatogenesis is markedly delayed in both importin $\alpha7^{\Delta IBB/\Delta IBB}$ and $\alpha7^{-/-}$ mice which is consistent with a dysfunction of Sertoli cells in both mouse lines.

Gene expression changes in α7$^{\Delta IBB/\Delta IBB}$ testis

To obtain a transcriptome-wide insight into the affected transcripts, pathways and upstream regulators after importin α7 depletion, we performed an RNAseq analysis on whole testes of WT, α7$^{\Delta IBB/\Delta IBB}$ and α7$^{-/-}$ mice in triplicate. A principal component analysis (PCA) on the gene aggregated transcript per million values depicts the transcriptome of α7$^{\Delta IBB/\Delta IBB}$ relative to WT and α7$^{-/-}$ mice (Fig. S4A). According to the PCA the transcriptomes of the former differ the most from the latter two along the first principal component (PC1), which is in accordance with the much more severe phenotype observed in α7$^{\Delta IBB/\Delta IBB}$ compared to α7$^{-/-}$ mice. A log likelihood test between the α7$^{\Delta IBB/\Delta IBB}$ and the WT transcriptome revealed 112 significantly regulated genes, with *Kpna6* significantly downregulated in the former (p-value: $3*10^{-5}$; effect size: -1.51, Fig. 9A; Table S1). Contrary to this and in line with the mild phenotype and the PCA, we found only 20 differentially regulated genes between WT and α7$^{-/-}$ mice, with *Kpna6* showing no significance in differential expression (Table S1). Therefore, we concentrated our analyses on the comparison of α7$^{\Delta IBB/\Delta IBB}$ and WT testes. We next performed a gene set enrichment analysis (GSEA) based on the gene effect size differences between the WT and α7$^{\Delta IBB/\Delta IBB}$ condition using the biological processes from the Gene Ontology (GO). Upregulated GO terms in α7$^{\Delta IBB/\Delta IBB}$ are related to cell migration, extracellular matrix and development processes, while cilia, flagellum and sperm related terms are downregulated due to the dysfunctional *Kpna6* gene (Fig 9B). To obtain an insight into the upstream transcription factors (TF), we tested the mouse regulon data from the DoroTheA library against the WT and α7$^{\Delta IBB/\Delta IBB}$ condition. In total there were 16 (20) TF whose putative activity was significantly up- (down-) regulated in α7$^{\Delta IBB/\Delta IBB}$ mice (Fig. 9C). While the upregulated TF were related to TNF-alpha signaling via NF-kB (adj. p-value=0.0008) and TGF-beta signaling (adj. p-value=0.02), Rfx2, a key regulator of mouse spermiogenesis was downregulated. To further test the prediction, we compared the differential gene regulation from α7$^{\Delta IBB/\Delta IBB}$ mice with testicular transcriptomes of Rfx2 knockout mice (Wu et al., 2016). The effect size and the direction of differential gene regulation for Rfx2 knockout and α7$^{\Delta IBB/\Delta IBB}$ mice relative to their wild type conditions are significantly correlated according to Spearman's rho statistic (p-value<$2.2*10^{-16}$). While both mouse lines share few upregulated genes (10% of Rfx2 KO; 7% of α7$^{\Delta IBB/\Delta IBB}$), 40% of the genes that were downregulated in α7$^{\Delta IBB/\Delta IBB}$, were also downregulated in Rfx2 knockout (Fig. 9D, Table S2). A GSEA of the downregulated pathways in Rfx2 knockout and α7$^{\Delta IBB/\Delta IBB}$ mice depicted similar effects on cilium, its assembly, microtubule- and sperm motility-related processes (Fig. 9E, Table S3). However, RFX2 localization in the testis did

not show abnormalities in $\alpha7^{\Delta IBB/\Delta IBB}$, being strongly expressed in nuclei of step 2-3 round spermatids, while the protein localizes to a distinct spot in the nuclei of step 4-8 round spermatids before disappearing when elongation starts (Fig. S4B). These data indicate that RFX2 is normally expressed in $\alpha7^{\Delta IBB/\Delta IBB}$ mice, but its activity on target genes seems to be impaired in the absence of importin α7.

Downregulation of protamines and transition proteins in round spermatids and impaired histone-protamine exchange in $\alpha7^{\Delta IBB/\Delta IBB}$ mice

Since analysis of the altered gene expression in $\alpha7^{\Delta IBB/\Delta IBB}$ mice suggested the strongest impact on postmeiotic events, we performed a detailed microscopic study of sperm maturation in the testis. While spermatid elongation started regularly in stage IX seminiferous tubules of $\alpha7^{\Delta IBB/\Delta IBB}$ mice, the subsequent steps were characterized by abnormal nuclear shaping of elongating spermatids and mature step15-16 sperms were absent in $\alpha7^{\Delta IBB/\Delta IBB}$ mice (Fig. 10). Together with the reduced number of spermatozoa and abnormal morphology of epididymal sperms in $\alpha7^{\Delta IBB/\Delta IBB}$ mice this suggested that spermiogenesis was severely affected by importin α7 deficiency, confirming the results of gene expression analysis. We next tested whether the regulation of postmeiotic factors, that are necessary for sperm maturation, is mediated by importin α7. The analysis of gene expression in whole testis had already shown a slight downregulation of *Tnp1*, *Tnp2*, *Prm1* and *Prm2* (respective adj. p-values: 0.007, 0.06, 0.06, 0.02; Table S1). Real-time PCR analysis demonstrated that the mRNAs of these genes were significantly reduced in FACS-sorted isolated round spermatids of $\alpha7^{\Delta IBB/\Delta IBB}$ mice compared to WT and $\alpha7^{-/-}$ (Fig. 11A, S5). In contrast, other postmeiotic key genes were not significantly affected in $\alpha7^{\Delta IBB/\Delta IBB}$ mice (Fig. 11A). Moreover, Western blot of chromatin-bound proteins showed that TNP2 was drastically decreased in the testes of $\alpha7^{\Delta IBB/\Delta IBB}$ mice (Fig. 11B). Although TNP1 and TNP2 were correctly localized in elongating spermatids starting at step9 (data not shown), we found a prolonged persistence of these two proteins in $\alpha7^{\Delta IBB/\Delta IBB}$ spermatids. In WT and importin $\alpha7^{-/-}$ testes, TNP1 cannot be found in tubules later than stage I, and TNP2 is not expressed past stage III, however, we constantly found TNP1-positive sperms until stage III tubules und expression of TNP2 was even found in sperms of stage VIII (and IX, residual sperms) tubules (Fig.11C, D). Taken together these data show that the expression of protamines and transition proteins is markedly reduced and that protamine-histone exchange is severely disturbed in mice lacking importin α7.

Analysis of chromatin remodeling and presence of transcription factors in α7$^{\Delta IBB/\Delta IBB}$ mice

Next we investigated the tremendous remodeling of chromatin that takes place during spermatid development, as this process is dependent on proteins that enter the nucleus of round and elongating spermatids. Analysis of histone H3 2- and 3-methylation as well as hyperacetylation of histone H3 (K9 and K14) and H4 (K8 and K12) did not reveal any differences of α7$^{\Delta IBB/\Delta IBB}$ and WT spermatids (data not shown). Moreover, we observed regular appearance of DNA double strand breaks detected by γH2AX labelling (Fig. 7B).

The significant reduction in gene expression of *Tnp1, Tnp2, Prm1* and *Prm2* may result from impaired expression or nuclear translocation of TFs. In mice, the transcriptional activation of these genes is mainly regulated by CREM (Mali et al., 1989; Nantel et al., 1996). WT testis showed a normal expression and localization of CREM in round spermatids step2-8 (Fig. S6) and with onset of elongation the CREM expression started to decline. However, no major changes in CREM expression and localization could be observed in α7$^{\Delta IBB/\Delta IBB}$ testis (Fig. S6), suggesting that nuclear import of CREM is unaffected.

The transcriptional regulator BRWD1 has been shown to be essential for spermiogenesis (Pattabiraman et al., 2015). Being part of a postmeiotic transcriptional activator complex, BRWD1 binds to acetylated lysine residues of histones, causing transcriptional activation. Immunofluorescence of BRWD1 revealed striking differences in its expression in α7$^{\Delta IBB/\Delta IBB}$ testes compared to WT and α7$^{-/-}$ testes. While in WT and α7$^{-/-}$ testes, positive signals localized to spots in the cytoplasm could be found in paraffin embedded testis sections in step9 elongating spermatids and in stage IV-VI tubules, no BRWD1 signal was found in α7$^{\Delta IBB/\Delta IBB}$ testis (Fig. 12). As the signals tended to be very subtle in paraffin sections, immunostaining was repeated in snap-frozen sections, confirming very clearly the spotty pattern of expression of BRWD1 in WT and α7$^{-/-}$, but not in α7$^{\Delta IBB/\Delta IBB}$ testes (Fig. S7A). Since quantification of BRWD1 by Western blots did not show a significant difference in whole testis extracts (Fig. S7B), we suggest that the intracellular localization of the protein is affected by the absence of importin α7.

Discussion

We used two different knockout mouse models lacking functional importin α7 either in all cells of the testis (α7$^{\Delta IBB/\Delta IBB}$) or expressing it only in germ cells (α7$^{-/-}$) to analyze the biological function of importin α7 during spermatogenesis and showed for the first time that

importin α7 in germ cells is essential for mammalian male fertility. These findings are in accordance with the phenotype of fruit flies lacking importin α1, which is the one (of three) importin α paralogs in *D. melanogaster* with the highest similarity to mouse importin α7. Importin α1 of *D. melanogaster* is essential for spermatogenesis and depletion leads to its full arrest with spermatocytes exhibiting abnormal nuclear shape (Ratan et al., 2008). However, the molecular mechanisms by which *D. melanogaster* importin α1 exerts its effects on male fertility have not been assessed yet.

Kpna6 mRNA is expressed in isolated pachytene spermatocytes and round spermatids (Holt et al., 2007; Major et al., 2011; Shima et al., 2004), and it is upregulated during the first spermatogenesis wave: a first increase takes place from postnatal day 10 to day 20, when spermatocytes progress into late pachytene stage; and a second increase occurs from postnatal day 20 to day 30, when round spermatids enrich (Major et al., 2011; Namekawa et al., 2006). The importin α7 protein expression pattern during spermatogenesis detected by immunohistochemistry in our current report is consistent with these data. Additionally, microarray data had shown that *Kpna6* mRNA is moderately expressed in cultured Sertoli cells isolated from postnatal day 16 to day 18 testes (Holt et al., 2007; Shima et al., 2004), while in adult testis, *Kpna6* mRNA was not detected in Sertoli cells by *in situ* hybridization (Hogarth et al., 2006). However, our present study shows, that importin α7 is also highly expressed in the nuclei of Sertoli cells throughout all stages of the seminiferous epithelium in the adult testis.

Studies of other importin α isoforms in adult mouse testis have shown stage- and cell type-specific expression of importin α1 α3, and α4 (Miyamoto et al., 2012). Our own comprehensive studies revealed, that importin α7 is the only importin α isoform expressed in elongating spermatids (data not shown). Moreover, we detected a massive increase in importin α7 expression in late round and early elongating spermatids that has not been seen for any other importin α subtype. The infertility phenotype of importin α7-deficient mice underlines the hypothesis that this protein has unique functions in spermatogenesis, and other importin α subtypes cannot compensate for its absence.

One of the main findings of our present work is that importin α7 has two different functions during spermatogenesis depending on its two localizations in Sertoli cells and in developing sperms. The use of two different importin α7-deficient mouse lines with distinct expression patterns in these cell types allowed us to discriminate between these two functions as both lines display distinct phenotypes. The $\alpha7^{\Delta IBB/\Delta IBB}$ mice are infertile and are characterized by the absence of the full-length protein in Sertoli cells and developing sperms. The $\alpha7^{-/-}$ mice are

fertile and produce sperms which can be clearly attributed to a rescued expression of the protein in developing sperms based on a germ cell-specific promoter in the *Kpna6* gene. The utilization of a germ cell-specific promoter is a well-known mechanism and has been shown for a variety of transcripts encoding for proteins such as angiotensin converting enzyme, c-abl, proopiomelanocortin, or ß-galactosyltransferase (Hecht, 1998). In WT and $\alpha7^{-/-}$ mice, germ cells produce *Kpna6* mRNA by using an alternative exon 1A with a germ cell specific 5'-untranslated region, suggesting differential transcriptional control mechanisms for *Kpna6* in these cells. However, the absence of importin α7 in Sertoli cells seems to account for a partially reduced sperm count. This finding could be confirmed by intercrossing of both lines, producing compound heterozygous offspring, which also displayed a reduced sperm count but were fertile. This provides clear evidence that the partial sperm count reduction can be attributed to the Sertoli cell-related phenotype, as the compound heterozygous mice represent a rescue of the infertile $\alpha7^{\Delta IBB/\Delta IBB}$ mice with expression of the protein in germ cells, but not in Sertoli cells.

We revealed several alterations in importin α7-deficient Sertoli cells which may explain this effect. First, we observed reduced nuclear AR in Sertoli cells of both mutant mouse lines. It has been shown that ligand-dependent nuclear import is crucial for the function of AR (Becker et al., 2000; Kawate et al., 2005; Nakauchi et al., 2007; Thomas et al., 2004), and its nuclear import is importin α/ß dependent (Cutress et al., 2008; Kaku et al., 2008). Mice with Sertoli cell-specific ablation of the AR (SCARKO) exhibit defective Sertoli cell polarization and nuclear position in the tubules, and progress through meiosis is disturbed with increased rate of apoptosis (Meng et al., 2011; Meng et al., 2005; Willems et al., 2010). Increased permeability of the BTB and downregulation of *Cldn3*, are typically found in SCARKO mice. Similar alterations were found in $\alpha7^{\Delta IBB/\Delta IBB}$ mice and partly in $\alpha7^{-/-}$ animals, but the effects were less pronounced. Most AR-dependent genes were normally expressed and the observed decrease in *Cldn3* mRNA levels in $\alpha7^{\Delta IBB/\Delta IBB}$ mice may be at least partially due to the loss of germ cells, in which this gene is also expressed (Chihara et al., 2013). Secondly, we found that Sertoli cells of both mutant lines display abnormal organization of the intermediate filament vimentin. While vimentin is stretched across the Sertoli cell cytosol in WT testis, both mutant mouse lines showed a concentration around the Sertoli cell nucleus with no extensions. Similar findings have been found in mice with a defective cytoplasmic dynein 1 heavy chain and in mice that have been depleted of RAPTOR, a key component of mTORC1 (Wen et al., 2018; Xiong et al., 2018). However, in both of these mouse lines, the phenotype included a severe disorganization of actin and microtubules, which we could not detect,

excluding major morphological changes of Sertoli cell cytoplasm which still stretched out into the tubular lumen.

Despite these relatively minor alterations in Sertoli cells lacking importin α7 the dynamic remodeling of the BTB during stages VII and VIII, which allows preleptotene spermatocytes the passage through the barrier (Bremner et al., 1994; Dym and Fawcett, 1970), seems to be impaired in $\alpha7^{\Delta IBB/\Delta IBB}$ and $\alpha7^{-/-}$ testes. We observed a relative reduction in leptotene/zygotene spermatocytes of about 25% in both lines which would be consistent with a meiotic delay due to a prolonged leptotene/zygotene phase as it had been observed in *Cldn3* knockdown mice (Chihara et al. 2013). Although both mutant mouse lines exhibit a loss of leptotene/zygotene spermatocytes, only $\alpha7^{\Delta IBB/\Delta IBB}$ mice show an even more pronounced loss of pachytene spermatocytes and round spermatids. As in pachytene spermatocytes in contrast to leptotene/zygotene spermatocytes importin α7 mRNA is already detectable (Holt et al., 2007; Major et al., 2011; Shima et al., 2004), low levels of protein might be crucial from this developmental stage on , explaining the loss of these postmeiotic cell types.

The retardation in the first wave of spermatogenesis was confirmed by detailed analyses in 21 days old testes. This delay fits to previous reports of importin α7 being upregulated from postnatal day 10, suggesting a very specific role at this time point (Major et al., 2011; Namekawa et al., 2006). Since both mouse lines are affected, we conclude that the defects in Sertoli cell function are responsible for this phenotype.

Multiple molecular events have to occur for a round spermatid to become a mature sperm. These events include chromatin condensation, reorganization of the spermatid nucleus, formation of an acrosome and assembly of a sperm tail (Sassone-Corsi, 2002). It has been shown that a number of postmeiotic proteins including TNP1 and TNP2, PRM1 and PRM2, MEiG1, ODF1, JHDM2A, ACT, and CAPZA3 (encoded by *Gsg3*), are important for spermiogenesis (Geyer et al., 2009; Kotaja et al., 2004; Liu et al., 2010; Okada et al., 2007; Salzberg et al., 2010; Yang et al., 2012; Zhang et al., 2009). The transition from round spermatids to mature spermatozoa was severely affected in $\alpha7^{\Delta IBB/\Delta IBB}$ mice. Spermiogenesis requires extensive chromatin condensation which is achieved by replacement of histones by TNP1 and TNP2 and subsequently by PRM1 and PRM2. Accordingly, the genetic ablation of transition proteins or protamines causes defective spermiogenesis (Cho et al., 2001; Yu et al., 2000; Zhao et al., 2004; Zhao et al., 2001) comparable to the phenotype of $\alpha7^{\Delta IBB/\Delta IBB}$ males. By RNAseq we found that importin α7 deficiency reduced *Tnp1*, *Tnp2*, *Prm1*, and *Prm2* expression in the testis. As the analysis of whole testis RNA bears the risk of different cellularity between the three mouse lines, we extended our study using FACS-sorted round

spermatids and here, the reduced expression of *Tnp1*, *Tnp2*, *Prm1*, and *Prm2* was even more pronounced. Moreover, total chromatin-bound TNP2 was markedly reduced in testes of $\alpha7^{\Delta IBB/\Delta IBB}$ mice as assessed by Western blot. In addition, we detected a prolonged presence of transition proteins in spermatids of $\alpha7^{\Delta IBB/\Delta IBB}$ mice, suggesting that importin α7 is not only essential for the expression of TNPs and PRMs but also for histone/protamine exchange.

The transcriptional regulator BRWD1 has been shown to be critical for spermiogenesis (Pattabiraman et al., 2015). Although a distinct pathway has not been found yet, the reduced transcription of postmeiotic genes, including *Tnp1*, *Tnp2*, *Prm1*, and *Prm2*, in *Brwd1*-defective testes has been suggested to cause male infertility. By immunohistochemistry we found a spotty pattern of BRWD1 localization in wild-type and $\alpha7^{-/-}$ testes which was absent in $\alpha7^{\Delta IBB/\Delta IBB}$ testes, while the amount of the protein was indistinguishable between the strains. These data render BRWD1 a possible mediator of the observed impairments in transition protein and protamine expression in $\alpha7^{\Delta IBB/\Delta IBB}$ testes.

A GSEA of the RNAseq data clearly indicated a downregulation of cilium- and sperm motility-related processes in $\alpha7^{\Delta IBB/\Delta IBB}$ mice, corroborating the finding of defective spermiogenesis. The analysis of putative TFs singled out a downregulation of RFX2 gene targets. While *Rfx2* itself was not differentially regulated, its targets related to cilium, axoneme, microtubule and sperm motility were, which was evident from a comparison of our RNAseq data to a testis transcriptome of Rfx2 knockout mice (Wu et al., 2016). Although immunohistochemical analysis of RFX2 in testis did not reveal a differential localization of the protein, it might be possible, that its posttranslational modification is disturbed or that a cofactor that has yet to be determined, is needed for effective transcription.

In the present study we have shown for the first time that importin α7 is essential for mammalian male fertility. We revealed two cell types in which the protein is functionally important in the testis. In Sertoli cells its deficiency causes alterations in AR and vimentin localization, and in BTB dynamics leading to a delay in spermiogenesis. At the level of round spermatids importin α7 is the main expressed α-importin and its deficiency severely affects the activity of RFX2, the localization of BRWD1, and the expression of transition proteins and protamines as well as the histone/protamine exchange. These effects contribute to the massive loss of elongating spermatids and the complete male infertility observed in $\alpha7^{\Delta IBB/\Delta IBB}$ mice. However, further investigations have to be performed to identify all the cellular and molecular mechanisms involved in the complex phenotype of infertility observed in importin α7 deficient mice.

Materials and Methods

Animals – Importin $\alpha7^{-/-}$ and $\alpha7^{\Delta IBB/\Delta IBB}$ mice were generated as described previously (Rother et al., 2011). Animals were backcrossed for 10 generations to C57Bl6/N background. All experiments were performed according to national and institutional guidelines and were approved by the relevant authority [Landesamt für Gesundheit und Soziales Berlin, Germany].

Western blot – Mouse testes were collected and homogenized in RIPA-Buffer supplemented with protease inhibitor cocktail (Sigma-Aldrich, St. Louis, USA). Following sonication and centrifugation, protein concentrations in the tissue extracts were measured by using Bicinchoninic Acid Solution / Coppersulfate Solution 50:1 (Sigma-Aldrich, St. Louis, USA). 40 µg of total protein was separated by SDS-PAGE. After the transfer of proteins, the PVDF membrane was blocked by Odyssey blocking solution (LiCor, Bad Homburg, Germany) and subsequently incubated with primary antibodies at 4°C overnight. On the next day, the membrane was incubated with an IRDye- coupled secondary antibody for 1 h at room temperature and detection was performed using the Odyssey Infrared Scanner (LiCor, Bad Homburg, Germany). Signals were quantified using the Odyssey Infrared Scanner software (LiCor, Bad Homburg, Germany). The generation of C-terminal and N-terminal antibodies against importin α7 was accomplished using standard protocols and has been described previously (Kohler et al., 1999). The complete list of antibodies and conditions is found in supplemental data (Table S4). For quantifications, at least 3 independent experiments were performed.

RNA-isolation, reverse transcription and PCR – Tissue was homogenized in trizol and extracted with chloroform, subsequently precipitated in isopropanol and washed with 70% ethanol. The pellet was dried and resuspended in DEPC water. Then RNA was digested with DNAse I, and 2 µg of digested RNA was subjected to reverse transcription using a standard protocol. PCR was performed using 10 ng of cDNA, the used primers are listed in supplemental data (Table S5).

Testosterone measurement – Blood samples were collected from 10-weeks-old mice by cardiac puncture. Serum samples were prepared as described earlier (Jeyaraj et al., 2005). The concentrations of testosterone in the serum samples were measured by using a Testosterone EIA kit (Cayman Chemical Company, Michigan, USA).

Histological analysis – Testis and Epididymis were fixed in neutral buffered 4% formalin. After fixation, tissues were dehydrated in increasing concentrations of ethanol, embedded in paraffin wax, and sectioned at a thickness of 5 µm. Sections were deparaffinised, rehydrated and stained with hematoxylin and eosin according to standard protocols. For quantification of diameters of seminiferous tubules, images of H&E stained testis sections (5 animals per group) were taken using Keyence microscope (Keyence, Bioreva BZ-9000, Germany) and analyzed; 30 tubules per animal were measured using ImageJ software.

Epididymal sperm count – Sperm count was performed as described previously (Liu et al., 2010; Wu et al., 2000). Briefly, one caudal epididymis was used for histological examination, and the other was minced in 1 ml of PBS. Sperms were allowed to disperse into solution by incubating for 5 min at room temperature. An aliquot of the sperm/saline mixture was then counted in a hemocytometer. The hemocytometer count was multiplied by appropriate volume and dilution factors to give a total cauda epididymal sperm count.

Immunohistochemical analysis – For IF staining sections underwent deparaffination followed by rehydration and antigen retrieval using either citrate buffer pH6 or Tris-EDTA buffer pH9 for 20 minutes, wherever appropriate. The sections were then treated with 10% normal donkey serum for 1h at room temperature and subsequently incubated with primary antibody overnight at 4°C. On the next day, sections were washed with PBS, incubated with secondary antibody for 2 h at room temperature, washed again with PBS and incubated for 1 h at room temperature with peanut agglutinin (PNA), subsequently washed again and embedded in mounting medium containing DAPI (Vectashield, Vector Laboratories/Biozol, Germany). Whenever needed, the immunostaining was performed on 10 µm thick frozen sections of testis fixed in neutral buffered 4% formalin. The complete list of antibodies and conditions is found in supplemental data (Table S4). Images of stained tissue sections were taken using a fluorescence microscope (Keyence, Bioreva BZ-9000, Germany) or a confocal fluorescence microscope (Leica TCS SPE). For cell counts, at least 100 seminiferous tubules of 3-8 mice per group were analyzed using ImageJ software.

Counting of developmental steps of germ cells – Spermatogonia were counted based on their positive staining for Sall4, the histogram shows the counts for BrdU-labelled S-phase preleptotene spermatocytes (only stage VII and VIII tubuli were used for calculation). For counting of leptotene/zygotene spermatocytes their intense expression of γH2AX was used as

marker. Pachytene spermatocytes were counted based on their nuclear shape and chromatin (DAPI) staining and their position in the tubuli.

Determination of apoptosis by TUNEL staining – Apoptosis in tissue sections of mouse testis was analyzed by TUNEL staining using an *in situ* cell death detection kit-Fluorescein (# 11684795910, Merck). In brief, paraffin embedded testis sections were deparaffinized and rehydrated, antigen retrieval was performed using citrate buffer pH 6.0 for 10 min. Unspecific bindings were blocked using 10% normal donkey serum for 30 min. The sections were then incubated for 90 min at 37°C with TUNEL reaction mixture prepared according to the manufacturer's protocol. The sections were washed in 1x PBS and incubated with PNA for 1h at room temperature, washed and coverslipped with mounting medium containing DAPI. The slides were visualized under a Keyence microscope (Keyence, Germany). The number of apoptotic cells was counted per entire section using imageJ.

Quantitative realtime PCR – Total RNA was extracted from WT, $\alpha7^{-/-}$ and $\alpha7^{\Delta IBB/\Delta IBB}$ testes and FACS sorted germ cells using RNeasy Mini Kits (Qiagen, Hilden, Germany). First-strand DNA synthesis was performed using M-MLV Reverse Transcriptase (Invitrogen, Darmstadt, Germany) and random primers according to the manufacturer's instructions. Quantitative PCR was performed using Go Taq (Promega, Mannheim, Germany) on an IQ 5 Multicolour Realtime PCR Detection System (Bio-Rad laboratories, München, Germany). Relative gene expression was calculated using the ΔΔCt method with *Gapdh* as normalizing gene. Primer sequences are listed in supplemented data (Table S5).

Autoantibody detection – Autoantibodies against sperm proteins were detected as described previously (Meng et al., 2011). Briefly, blots with testicular proteins of two months old WT mice were incubated with a 1:50 dilution of either WT, $\alpha7^{\Delta IBB/\Delta IBB}$ or $\alpha7^{-/-}$ mutant sera overnight at 4°C. Primary antibodies were detected with an IRDye coupled secondary anti-mouse antibody for 1 h at room temperature and detection was performed using the Odyssey Infrared Scanner (LiCor, Bad Homburg, Germany).

Biotin-labelling of blood-testis barrier – Mice were sacrificed by cervical dislocation and testis were carefully pulled out of the body without extracting them. 50 µl of 1 mM $CaCl_2$ containing 10 mg/ml biotin (EZ-Link Sulfo-NHS-LC-Biotin, Pierce, Dallas, USA) were injected with a 0.4 mm needle into one testis. As a control, the second testis was injected with

50 µl of 1 mM $CaCl_2$ only. After 30 min of distribution of the injected solution via diffusion the testes were dissected and snap frozen in Tissue-Tek OCT compound (Sakura Finetek, Netherlands). 15 µm cryoslices were cut, mounted on glass slides and fixed with 4% PFA for 15 min. After washing, the sections were incubated with streptavidin-Cy5 directly, coversliped and observed under a fluorescence microscope (Keyence, Bioreva BZ-9000).

BrdU injection – To analyze proliferation of germ cells, animals received two intraperitoneal injections of bromodeoxyuridine (BrdU; 50 mg/kg body weight dissolved in 0.9% NaCl; Sigma-Aldrich) 2 h apart and were sacrificed 2 h after the second injection.

RNAsequencing

A total amount of 1 µg RNA per sample was used as input material for the RNA sample preparations. Sequencing libraries were generated using NEBNext® UltraTM RNA Library Prep Kit for Illumina® (NEB, USA) following manufacturer's recommendations and index codes were added to attribute sequences to each sample. Briefly, mRNA was purified from total RNA using poly-T oligo-attached magnetic beads. Fragmentation was carried out using divalent cations under elevated temperature in NEBNext First Strand Synthesis Reaction Buffer (5X). First strand cDNA was synthesized using random hexamer primer and M-MuLV Reverse Transcriptase (RNase H-). Second strand cDNA synthesis was subsequently performed using DNA Polymerase I and RNase H. Remaining overhangs were converted into blunt ends via exonuclease/polymerase activities. After adenylation of 3' ends of DNA fragments, NEBNext Adaptor with hairpin loop structure were ligated to prepare for hybridization. In order to select cDNA fragments of preferentially 150~200 bp in length, the library fragments were purified with AMPure XP system (Beckman Coulter, Beverly, USA). Then 3 µl USER Enzyme (NEB, USA) was used with size-selected, adaptor- ligated cDNA at 37 °C for 15 min followed by 5 min at 95 °C before PCR. PCR was performed with Phusion High-Fidelity DNA polymerase, Universal PCR primers and Index (X) Primer. At last, PCR products were purified (AMPure XP system) and library quality was assessed on the Agilent Bioanalyzer 2100 system. Fastq reads were pseudo-aligned to the mm10 genome assembly using kallisto (version 0.46) and transcript read counts were aggregated to Ensembl Gene IDs for further analysis. Differential gene expression analysis was performed via the R library sleuth (Pimentel et al., 2017). Significance and effect sizes of differential gene regulation were calculated from the likelihood ratio and the Wald test, respectively, as implemented in the sleuth package. GO term and pathway enrichment analyses were performed based on the

effect size between the WT and knockdown strains using the generally applicable GSEA GAGE, which determines whether a set of genes is systematically up- or downregulated as a whole (Luo et al., 2009). For gene set definitions, we used the Molecular Signatures Database (MSigDB) from the R msigdf package (Version 7.1) (Liberzon et al., 2015). Gene sets with less than 3 or those with more than 500 members were discarded for statistical robustness and biological interpretation. Putative transcription factor activity from RNA-seq data was assessed per pseudo timepoint against healthy controls using the mouse gene set resource DoRothEA v1, which provides a curated collection of transcription factor and target genes interactions (the regulon) from different sources (Garcia-Alonso et al., 2019). Only interactions with high, likely, and medium confidence (levels A, B, C) were considered. Regulons were statistically evaluated using the R package *viper* (v1.22.0; row-wise t-tests) (Alvarez et al., 2016). Only regulons having at least 15 expressed gene targets were considered. The RNAseq data are available through Gene Expression Omnibus (GEO) under ID GSE160969 and can be accessed at https://www.ncbi.nlm.nih.gov/geo/query/acc.cgi?acc=GSE160969 using the token 'qxofaykwndszjix'.

Testicular single-cell suspensions – Cells were isolated according to a protocol of Getun et al. with slight modifications (Getun et al., 2011). Briefly, tunica albuginea was removed, and the seminiferous tubules were fragmented with scissors. The fragments were dissociated in dispase (BD Biosciences) with 10 U/ml DNAse I for 40 min at 37°C. After centrifugation, the pelleted tubules were resuspended in trypLE express enzyme (Life Technologies) with 10 U/ml DNAse I and incubated at 32°C for 20 min. The resulting whole cell suspension was successively washed with Gey's balanced salt solution (GBSS, Sigma-Aldrich). Then the cell pellet was resuspended in GBSS supplemented with 10% fetal calf serum and 10 U/ml DNAse I. The dissociated testis sample was then passed through a 40 µm GBSS pre-wetted disposable cell strainer. Final staining was performed by adding Hoechst 33342 (5 µg/ml) to the dissociated testis sample and incubating at 32°C for 1 h. Before analysis, propidium iodide (PI at 2 µg/ml) was added to exclude dead cells.

FACS sorting – FACS sorting was performed according to a slightly modified protocol of Bastos et al. (Bastos et al., 2005). Briefly, the enrichment of round spermatids was performed on a FACSAria III cell sorter from BD Biosciences. Live stained testicular cells were excited with a near UV laser (375 nm), the two parameters Hoechst blue (450/40 BP) and Hoechst red

(670 LP) were used to identify and sort. A sample of every sorting event was assessed for purity of round spermatids under a fluorescence microscope.

Extraction of chromatin-bound proteins – Extraction of basic nuclear proteins from mouse testis was performed according to Eckhardt (Eckhardt and Wang-Eckhardt, 2015). Briefly, one testis was homogenized in ice-cold NETN buffer, centrifuged at 12,000 x g for 10 min, resuspended in NETN buffer and centrifuged again. Then, the pellet was resuspended in 0.2 N HCl and incubated overnight at 4°C. After centrifugation at 12,000 x g for 10 min, the supernatant containing basic nuclear proteins was neutralized with 1 M Tris-HCl (pH 8.5) and protein concentration was determined.

Statistics – Statistical analysis was performed with Prism7 (GraphPad). Results are presented as means ± SEM. Significance was determined by using ANOVA (where 3 groups were compared) or the unpaired two-tailed Student's t test. For distribution of the genotype after heterozygous mating the binominal test was used. Given n-numbers in figure legends represent biological replicates. Significance was assumed for $p < 0.05$ (*, $p < 0.05$; **, $p < 0.01$; ***, $p < 0.001$; ****, $p < 0.0001$; n.s., not significant).

Acknowledgements

The authors wish to thank Anne Hahmann, Andrea Rodak and Madeleine Skorna-Nussbeck for technical assistance. We thank Laura Pelz and Fritz Rathjen for providing a BT-IgSF knockout mouse. We also thank Hans-Peter Rahn for help with FACS sorting of cells and the Advanced Light Microscopy technology platform of the MDC for technical support.

Competing interests

We declare no significant competing interests.

Funding

The work was partly supported by the DFG (BA 1374/21-1 and RO 4779/1-2).

References

Alvarez, M.J., Y. Shen, F.M. Giorgi, A. Lachmann, B.B. Ding, B.H. Ye, and A. Califano. 2016. Functional characterization of somatic mutations in cancer using network-based inference of protein activity. *Nature genetics*. 48:838-847.

Bastos, H., B. Lassalle, A. Chicheportiche, L. Riou, J. Testart, I. Allemand, and P. Fouchet. 2005. Flow cytometric characterization of viable meiotic and postmeiotic cells by Hoechst 33342 in mouse spermatogenesis. *Cytometry A*. 65:40-49.

Becker, M., E. Martin, J. Schneikert, H.F. Krug, and A.C. Cato. 2000. Cytoplasmic localization and the choice of ligand determine aggregate formation by androgen receptor with amplified polyglutamine stretch. *J Cell Biol*. 149:255-262.

Bellve, A.R., and W. Zheng. 1989. Growth factors as autocrine and paracrine modulators of male gonadal functions. *J Reprod Fertil*. 85:771-793.

Blanco-Rodriguez, J. 2009. γH2AX marks the main events of the spermatogenic process. *Microscopy research and technique*. 72:823-832.

Bremner, W.J., M.R. Millar, R.M. Sharpe, and P.T. Saunders. 1994. Immunohistochemical localization of androgen receptors in the rat testis: evidence for stage-dependent expression and regulation by androgens. *Endocrinology*. 135:1227-1234.

Celeste, A., S. Petersen, P.J. Romanienko, O. Fernandez-Capetillo, H.T. Chen, O.A. Sedelnikova, B. Reina-San-Martin, V. Coppola, E. Meffre, M.J. Difilippantonio, C. Redon, D.R. Pilch, A. Olaru, M. Eckhaus, R.D. Camerini-Otero, L. Tessarollo, F. Livak, K. Manova, W.M. Bonner, M.C. Nussenzweig, and A. Nussenzweig. 2002. Genomic instability in mice lacking histone H2AX. *Science*. 296:922-927.

Chihara, M., R. Ikebuchi, S. Otsuka, O. Ichii, Y. Hashimoto, A. Suzuki, Y. Saga, and Y. Kon. 2013. Mice stage-specific claudin 3 expression regulates progression of meiosis in early stage spermatocytes. *Biol Reprod*. 89:3.

Cho, C., W.D. Willis, E.H. Goulding, H. Jung-Ha, Y.C. Choi, N.B. Hecht, and E.M. Eddy. 2001. Haploinsufficiency of protamine-1 or -2 causes infertility in mice. *Nature genetics*. 28:82-86.

Clermont, Y. 1993. Introduction to the Sertoli cell. *The sertoli cell. Clearwater, FL: Cache River*.

Cutress, M.L., H.C. Whitaker, I.G. Mills, M. Stewart, and D.E. Neal. 2008. Structural basis for the nuclear import of the human androgen receptor. *J Cell Sci*. 121:957-968.

Dym, M., and D.W. Fawcett. 1970. The blood-testis barrier in the rat and the physiological compartmentation of the seminiferous epithelium. *Biol Reprod*. 3:308-326.

Eckhardt, M., and L. Wang-Eckhardt. 2015. A commercial human protamine-2 antibody used in several studies to detect mouse protamine-2 recognizes mouse transition protein-2 but not protamine-2. *Mol Hum Reprod*. 21:825-831.

Eddy, E.M., and D.A. O'Brien. 1998. Gene expression during mammalian meiosis. *Curr Top Dev Biol*. 37:141-200.

Garcia-Alonso, L., C.H. Holland, M.M. Ibrahim, D. Turei, and J. Saez-Rodriguez. 2019. Benchmark and integration of resources for the estimation of human transcription factor activities. *Genome Res*. 29:1363-1375.

Getun, I.V., B. Torres, and P.R. Bois. 2011. Flow cytometry purification of mouse meiotic cells. *J Vis Exp*.

Geyer, C.B., A.L. Inselman, J.A. Sunman, S. Bornstein, M.A. Handel, and E.M. Eddy. 2009. A missense mutation in the Capza3 gene and disruption of F-actin organization in spermatids of repro32 infertile male mice. *Developmental biology*. 330:142-152.

Hamer, G., H.L. Roepers-Gajadien, A. van Duyn-Goedhart, I.S. Gademan, H.B. Kal, P.P. van Buul, and D.G. de Rooij. 2003. DNA double-strand breaks and gamma-H2AX signaling in the testis. *Biol Reprod*. 68:628-634.

Hecht, N.B. 1998. Molecular mechanisms of male germ cell differentiation. *Bioessays*. 20:555-561.

Hermo, L., R.M. Pelletier, D.G. Cyr, and C.E. Smith. 2010. Surfing the wave, cycle, life history, and genes/proteins expressed by testicular germ cells. Part 1: background to spermatogenesis, spermatogonia, and spermatocytes. *Microscopy research and technique*. 73:241-278.

Hogarth, C.A., S. Calanni, D.A. Jans, and K.L. Loveland. 2006. Importin alpha mRNAs have distinct expression profiles during spermatogenesis. *Developmental dynamics : an official publication of the American Association of Anatomists*. 235:253-262.

Hogarth, C.A., D.A. Jans, and K.L. Loveland. 2007. Subcellular distribution of importins correlates with germ cell maturation. *Developmental dynamics : an official publication of the American Association of Anatomists*. 236:2311-2320.
Holt, J.E., J.D. Ly-Huynh, A. Efthymiadis, G.R. Hime, K.L. Loveland, and D.A. Jans. 2007. Regulation of Nuclear Import During Differentiation; The IMP alpha Gene Family and Spermatogenesis. *Current genomics*. 8:323-334.
Jeyaraj, D.A., G. Grossman, and P. Petrusz. 2005. Altered bioavailability of testosterone in androgen-binding protein-transgenic mice. *Steroids*. 70:704-714.
Johnson, L., D.L. Thompson, Jr., and D.D. Varner. 2008. Role of Sertoli cell number and function on regulation of spermatogenesis. *Anim Reprod Sci*. 105:23-51.
Kaku, N., K. Matsuda, A. Tsujimura, and M. Kawata. 2008. Characterization of nuclear import of the domain-specific androgen receptor in association with the importin alpha/beta and Ran-guanosine 5'-triphosphate systems. *Endocrinology*. 149:3960-3969.
Kawate, H., Y. Wu, K. Ohnaka, R.H. Tao, K. Nakamura, T. Okabe, T. Yanase, H. Nawata, and R. Takayanagi. 2005. Impaired nuclear translocation, nuclear matrix targeting, and intranuclear mobility of mutant androgen receptors carrying amino acid substitutions in the deoxyribonucleic acid-binding domain derived from androgen insensitivity syndrome patients. *The Journal of clinical endocrinology and metabolism*. 90:6162-6169.
Kohler, M., S. Ansieau, S. Prehn, A. Leutz, H. Haller, and E. Hartmann. 1997. Cloning of two novel human importin-alpha subunits and analysis of the expression pattern of the importin-alpha protein family. *FEBS Lett*. 417:104-108.
Kohler, M., C. Speck, M. Christiansen, F.R. Bischoff, S. Prehn, H. Haller, D. Gorlich, and E. Hartmann. 1999. Evidence for distinct substrate specificities of importin alpha family members in nuclear protein import. *Mol Cell Biol*. 19:7782-7791.
Kotaja, N., D. De Cesare, B. Macho, L. Monaco, S. Brancorsini, E. Goossens, H. Tournaye, A. Gansmuller, and P. Sassone-Corsi. 2004. Abnormal sperm in mice with targeted deletion of the act (activator of cAMP-responsive element modulator in testis) gene. *Proc Natl Acad Sci U S A*. 101:10620-10625.
Liberzon, A., C. Birger, H. Thorvaldsdóttir, M. Ghandi, J.P. Mesirov, and P. Tamayo. 2015. The Molecular Signatures Database (MSigDB) hallmark gene set collection. *Cell Syst*. 1:417-425.
Liu, Z., S. Zhou, L. Liao, X. Chen, M. Meistrich, and J. Xu. 2010. Jmjd1a demethylase-regulated histone modification is essential for cAMP-response element modulator-regulated gene expression and spermatogenesis. *The Journal of biological chemistry*. 285:2758-2770.
Luo, W., M.S. Friedman, K. Shedden, K.D. Hankenson, and P.J. Woolf. 2009. GAGE: generally applicable gene set enrichment for pathway analysis. *BMC Bioinformatics*. 10:161.
Macara, I.G. 2001. Transport into and out of the nucleus. *Microbiol Mol Biol Rev*. 65:570-594, table of contents.
Major, A.T., P.A. Whiley, and K.L. Loveland. 2011. Expression of nucleocytoplasmic transport machinery: clues to regulation of spermatogenic development. *Biochim Biophys Acta*. 1813:1668-1688.
Mali, P., A. Kaipia, M. Kangasniemi, J. Toppari, M. Sandberg, N.B. Hecht, and M. Parvinen. 1989. Stage-specific expression of nucleoprotein mRNAs during rat and mouse spermiogenesis. *Reproduction, fertility, and development*. 1:369-382.
Meng, J., A.R. Greenlee, C.J. Taub, and R.E. Braun. 2011. Sertoli cell-specific deletion of the androgen receptor compromises testicular immune privilege in mice. *Biol Reprod*. 85:254-260.
Meng, J., R.W. Holdcraft, J.E. Shima, M.D. Griswold, and R.E. Braun. 2005. Androgens regulate the permeability of the blood-testis barrier. *Proc Natl Acad Sci U S A*. 102:16696-16700.
Miyamoto, Y., P.R. Boag, G.R. Hime, and K.L. Loveland. 2012. Regulated nucleocytoplasmic transport during gametogenesis. *Biochim Biophys Acta*. 1819:616-630.
Nakauchi, H., K. Matsuda, I. Ochiai, A. Kawauchi, Y. Mizutani, T. Miki, and M. Kawata. 2007. A differential ligand-mediated response of green fluorescent protein-tagged androgen receptor in living prostate cancer and non-prostate cancer cell lines. *J Histochem Cytochem*. 55:535-544.
Namekawa, S.H., P.J. Park, L.F. Zhang, J.E. Shima, J.R. McCarrey, M.D. Griswold, and J.T. Lee. 2006. Postmeiotic sex chromatin in the male germline of mice. *Current biology : CB*. 16:660-667.

Nantel, F., L. Monaco, N.S. Foulkes, D. Masquilier, M. LeMeur, K. Henriksen, A. Dierich, M. Parvinen, and P. Sassone-Corsi. 1996. Spermiogenesis deficiency and germ-cell apoptosis in CREM-mutant mice. *Nature*. 380:159-162.
Okada, Y., G. Scott, M.K. Ray, Y. Mishina, and Y. Zhang. 2007. Histone demethylase JHDM2A is critical for Tnp1 and Prm1 transcription and spermatogenesis. *Nature*. 450:119-123.
Orth, J.M., G.L. Gunsalus, and A.A. Lamperti. 1988. Evidence from Sertoli cell-depleted rats indicates that spermatid number in adults depends on numbers of Sertoli cells produced during perinatal development. *Endocrinology*. 122:787-794.
Pattabiraman, S., C. Baumann, D. Guisado, J.J. Eppig, J.C. Schimenti, and R. De La Fuente. 2015. Mouse BRWD1 is critical for spermatid postmeiotic transcription and female meiotic chromosome stability. *J Cell Biol*. 208:53-69.
Peters, A.H., A.W. Plug, M.J. van Vugt, and P. de Boer. 1997. A drying-down technique for the spreading of mammalian meiocytes from the male and female germline. *Chromosome Res*. 5:66-68.
Pimentel, H., N.L. Bray, S. Puente, P. Melsted, and L. Pachter. 2017. Differential analysis of RNA-seq incorporating quantification uncertainty. *Nat Methods*. 14:687-690.
Ratan, R., D.A. Mason, B. Sinnot, D.S. Goldfarb, and R.J. Fleming. 2008. Drosophila importin alpha1 performs paralog-specific functions essential for gametogenesis. *Genetics*. 178:839-850.
Rother, F., T. Shmidt, E. Popova, A. Krivokharchenko, S. Hugel, L. Vilianovich, M. Ridders, K. Tenner, N. Alenina, M. Kohler, E. Hartmann, and M. Bader. 2011. Importin alpha7 is essential for zygotic genome activation and early mouse development. *PLoS One*. 6:e18310.
Russell, L.D. 1990. Histological and histopathological evaluation of the testis. Cache River Press, Clearwater, Fl.
Russell, L.D., and M.D. Griswold. 1993. The sertoli cell. Cache River Press Clearwater^ eFL FL.
Salzberg, Y., T. Eldar, O.D. Karminsky, S.B. Itach, S. Pietrokovski, and J. Don. 2010. Meig1 deficiency causes a severe defect in mouse spermatogenesis. *Developmental biology*. 338:158-167.
Sassone-Corsi, P. 2002. Unique chromatin remodeling and transcriptional regulation in spermatogenesis. *Science*. 296:2176-2178.
Shima, J.E., D.J. McLean, J.R. McCarrey, and M.D. Griswold. 2004. The murine testicular transcriptome: characterizing gene expression in the testis during the progression of spermatogenesis. *Biol Reprod*. 71:319-330.
Tejomurtula, J., K.B. Lee, S.K. Tripurani, G.W. Smith, and J. Yao. 2009. Role of importin alpha8, a new member of the importin alpha family of nuclear transport proteins, in early embryonic development in cattle. *Biol Reprod*. 81:333-342.
Thomas, M., N. Dadgar, A. Aphale, J.M. Harrell, R. Kunkel, W.B. Pratt, and A.P. Lieberman. 2004. Androgen receptor acetylation site mutations cause trafficking defects, misfolding, and aggregation similar to expanded glutamine tracts. *The Journal of biological chemistry*. 279:8389-8395.
Tsuji, L., T. Takumi, N. Imamoto, and Y. Yoneda. 1997. Identification of novel homologues of mouse importin alpha, the alpha subunit of the nuclear pore-targeting complex, and their tissue-specific expression. *FEBS Lett*. 416:30-34.
Walker, W.H. 2010. Non-classical actions of testosterone and spermatogenesis. *Philosophical transactions of the Royal Society of London. Series B, Biological sciences*. 365:1557-1569.
Wen, Q., E.I. Tang, W.Y. Lui, W.M. Lee, C.K.C. Wong, B. Silvestrini, and C.Y. Cheng. 2018. Dynein 1 supports spermatid transport and spermiation during spermatogenesis in the rat testis. *Am J Physiol Endocrinol Metab*. 315:E924-E948.
Willems, A., S.R. Batlouni, A. Esnal, J.V. Swinnen, P.T. Saunders, R.M. Sharpe, L.R. Franca, K. De Gendt, and G. Verhoeven. 2010. Selective ablation of the androgen receptor in mouse sertoli cells affects sertoli cell maturation, barrier formation and cytoskeletal development. *PLoS One*. 5:e14168.
Wu, J.Y., T.J. Ribar, D.E. Cummings, K.A. Burton, G.S. McKnight, and A.R. Means. 2000. Spermiogenesis and exchange of basic nuclear proteins are impaired in male germ cells lacking Camk4. *Nature genetics*. 25:448-452.

Wu, Y., X. Hu, Z. Li, M. Wang, S. Li, X. Wang, X. Lin, S. Liao, Z. Zhang, X. Feng, S. Wang, X. Cui, Y. Wang, F. Gao, R.A. Hess, and C. Han. 2016. Transcription Factor RFX2 Is a Key Regulator of Mouse Spermiogenesis. *Sci Rep*. 6:20435.

Xiong, Z., C. Wang, Z. Wang, H. Dai, Q. Song, Z. Zou, B. Xiao, A.Z. Zhao, X. Bai, and Z. Chen. 2018. Raptor directs Sertoli cell cytoskeletal organization and polarity in the mouse testis. *Biol Reprod*. 99:1289-1302.

Yang, K., A. Meinhardt, B. Zhang, P. Grzmil, I.M. Adham, and S. Hoyer-Fender. 2012. The small heat shock protein ODF1/HSPB10 is essential for tight linkage of sperm head to tail and male fertility in mice. *Mol Cell Biol*. 32:216-225.

Yu, Y.E., Y. Zhang, E. Unni, C.R. Shirley, J.M. Deng, L.D. Russell, M.M. Weil, R.R. Behringer, and M.L. Meistrich. 2000. Abnormal spermatogenesis and reduced fertility in transition nuclear protein 1-deficient mice. *Proc Natl Acad Sci U S A*. 97:4683-4688.

Zhang, Z., X. Shen, D.R. Gude, B.M. Wilkinson, M.J. Justice, C.J. Flickinger, J.C. Herr, E.M. Eddy, and J.F. Strauss, 3rd. 2009. MEIG1 is essential for spermiogenesis in mice. *Proc Natl Acad Sci U S A*. 106:17055-17060.

Zhao, M., C.R. Shirley, S. Mounsey, and M.L. Meistrich. 2004. Nucleoprotein transitions during spermiogenesis in mice with transition nuclear protein Tnp1 and Tnp2 mutations. *Biol Reprod*. 71:1016-1025.

Zhao, M., C.R. Shirley, Y.E. Yu, B. Mohapatra, Y. Zhang, E. Unni, J.M. Deng, N.A. Arango, N.H. Terry, M.M. Weil, L.D. Russell, R.R. Behringer, and M.L. Meistrich. 2001. Targeted disruption of the transition protein 2 gene affects sperm chromatin structure and reduces fertility in mice. *Mol Cell Biol*. 21:7243-7255.

Figures

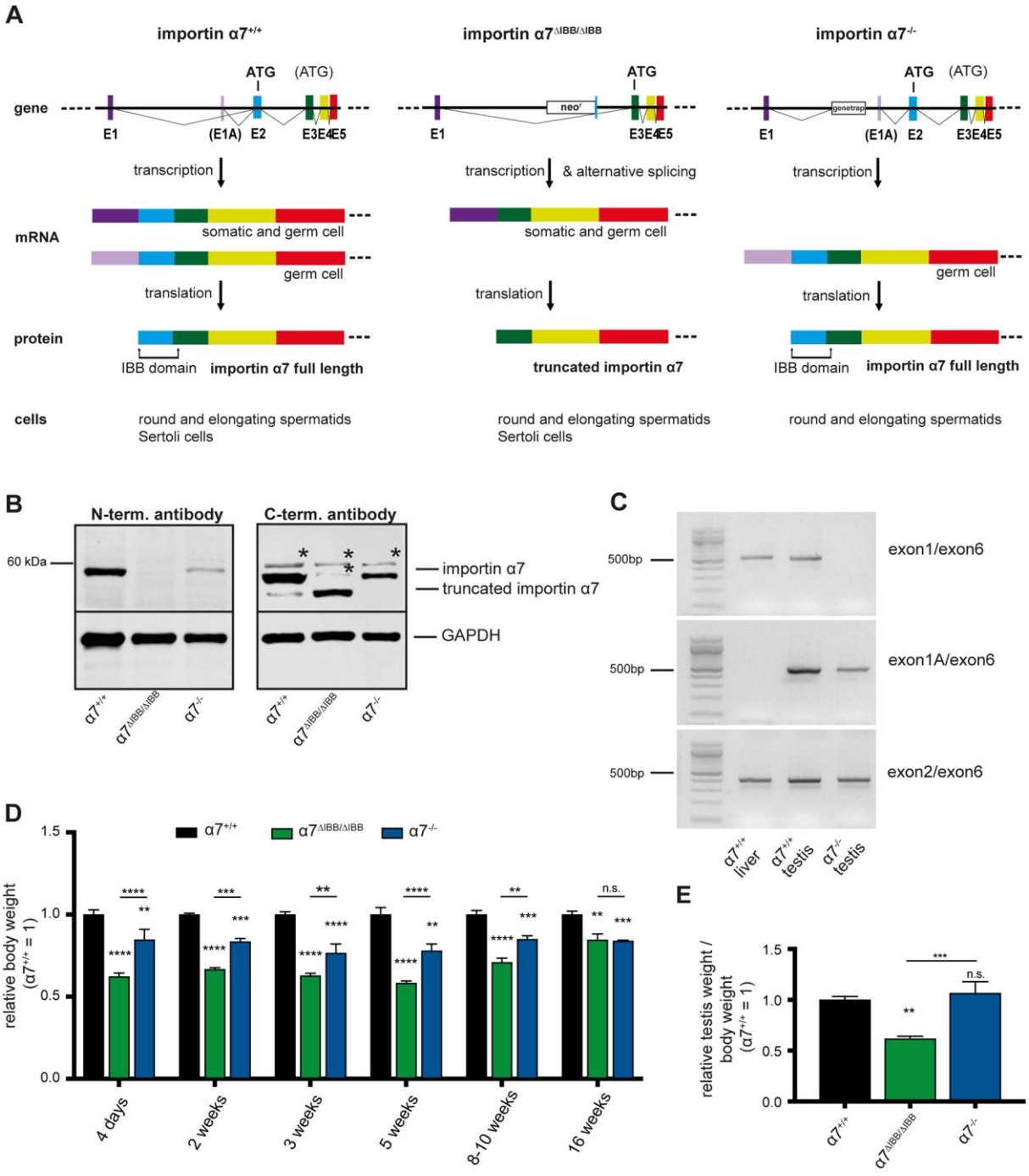

Fig. 1 Disruption of importin α7 causes growth retardation and reduced testis size. (A) Gene targeting strategy for $\alpha7^{\Delta IBB/\Delta IBB}$ and $\alpha7^{-/-}$ mice. In $\alpha7^{\Delta IBB/\Delta IBB}$, exon2 is replaced by a neomycin resistence (neo^r) cassette with a polyadenylation site (pA). Since transcription does not always stop at pA, a splicing variant is generated, carrying an *in frame* translational start site in exon 3, resulting in the formation of a truncated protein. In $\alpha7^{-/-}$ mice, a genetrap is located in intron1, leading to complete loss of the protein in most of the tissues. However, a

testis-specific exon1A (E1A) allows the generation of a germ cell-specific mRNA resulting in a full-length protein. (B) Western blot analysis of importin α7 expression in testes. The 58 kDa protein is absent in $\alpha7^{\Delta IBB/\Delta IBB}$ testes, while it can be detected in $\alpha7^{-/-}$ and WT testes (left). An importin $\alpha7^{\Delta IBB}$ protein which is about 10 kDa smaller than the full-length protein is found in the testis of $\alpha7^{\Delta IBB/\Delta IBB}$ mice (right). Asterisks mark unspecific cross-reactions of the antibody. (C) RT-PCR of WT liver, WT testis and $\alpha7^{-/-}$ testis using primer pairs spanning different exons of *Kpna6*. In WT liver and testis, a transcript spanning exon1 and exon6 can be detected, while it is absent in $\alpha7^{-/-}$ testis. WT testis, but not WT liver expresses a specific transcript using exon1A and this transcript can be detected in $\alpha7^{-/-}$ testis, too. All tested tissues express transcripts spanning exon2-6. (D) Relative body weight at various ages (n=6 per group). (E) Relative testis weight at 8-10 weeks of age (n=6 per group).

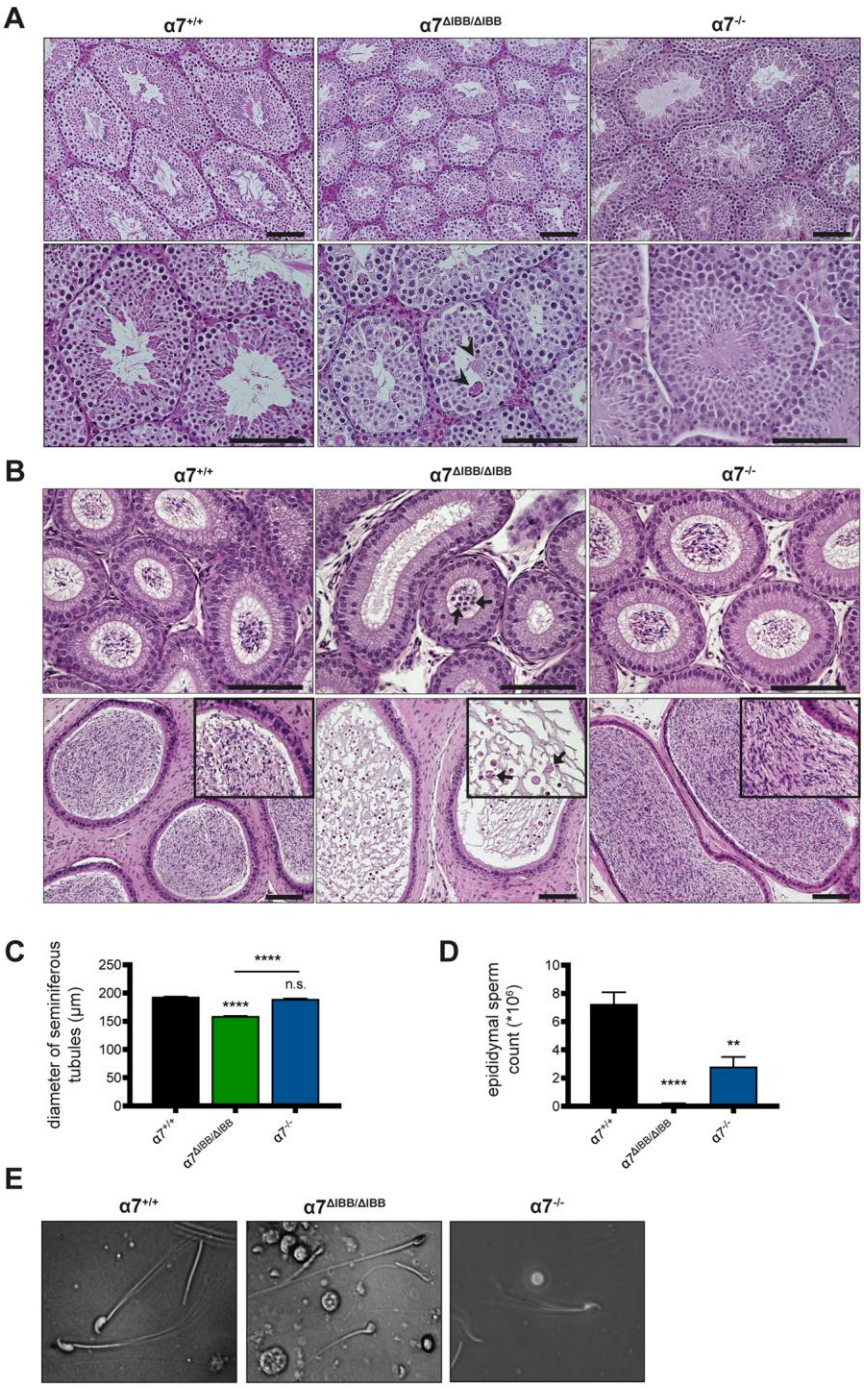

Fig. 2 Disruption of importin α7 causes oligozoospermia. (A, B) H&E staining of testis (A) and epididymis (B, upper lane: caput; lower lane: cauda) sections. Arrow heads in (A): multinucleated spermatid giant cells; arrows in (B): immature germ cells (upper lane), sloughed immature germ cells (lower lane). (C) Diameters of seminiferous tubules. (D) Epididymal sperm count ($\alpha7^{+/+}$: n=6, $\alpha7^{\Delta IBB/\Delta IBB}$: n=4, $\alpha7^{-/-}$: n=8). (E) Representative images of epididymal sperms from WT, $\alpha7^{\Delta IBB/\Delta IBB}$ and $\alpha7^{-/-}$ mice. Age of mice: 12-16 weeks. Scale bars: 100 µm.

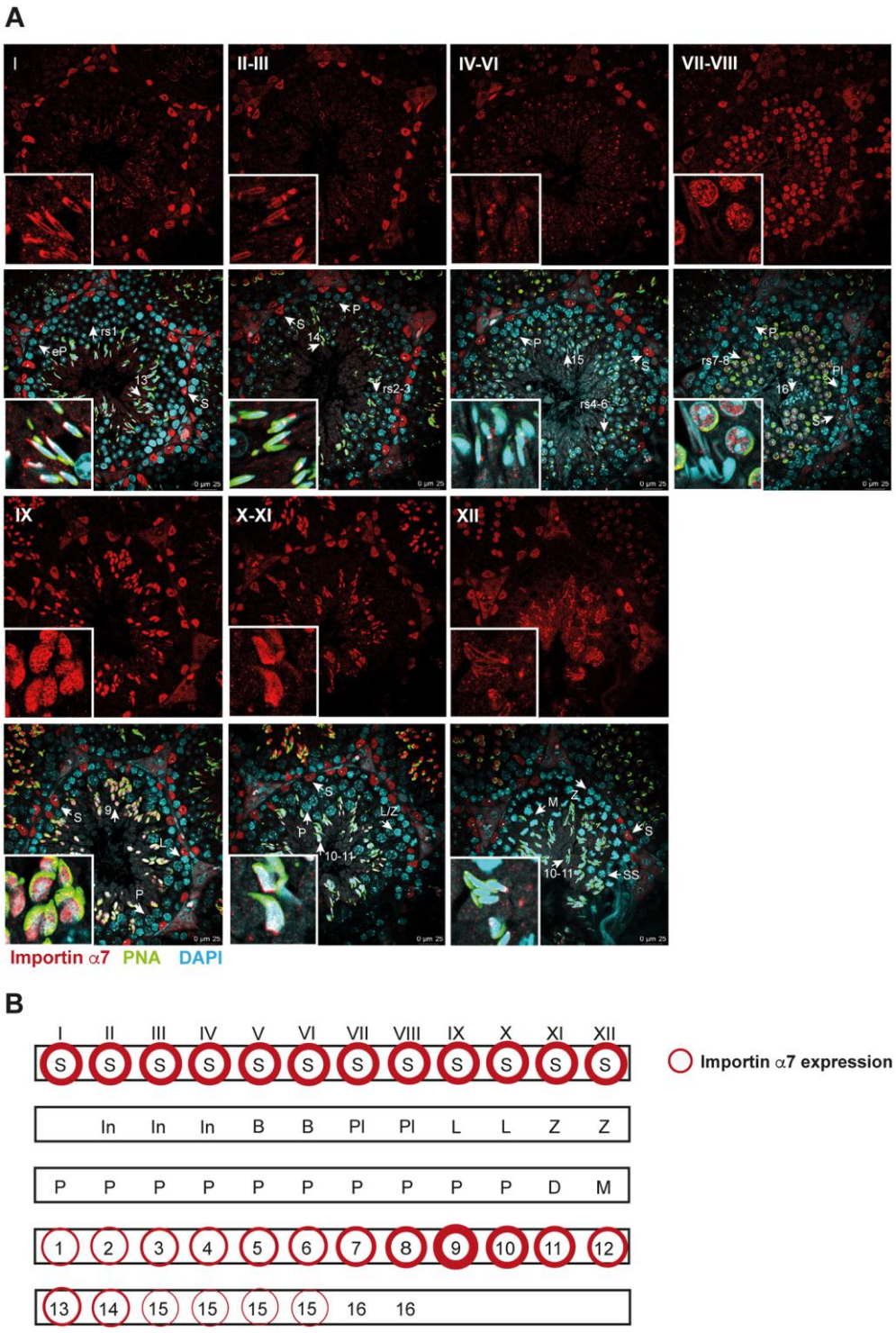

Fig. 3 Importin α7 is expressed in postmeiotic spermatids and Sertoli cells. (A) Immunohistochemistry of testis sections of adult mice (12-16 weeks) using an antibody against the C-terminus of importin α7 (red), counterstained with DAPI (blue) and PNA, labelling the acrosome (green). Roman numbers mark tubular stages. Scale bars: 25 µm. (B) Schematic image of importin α7-expressing cell types in mouse testis. S: Sertoli cell; Pl:

preleptotene spermatocyte; L: leptotene spermatocyte; L/Z: leptotene/zygotene spermatocyte; Z: zygotene spermatocyte; eP: early pachytene spermatocyte; P: pachytene spermatocyte; M: meiosis, SS: secondary spermatocyte; D: diakinesis spermatocyte; In: intermediate spermatogonium; B: type B spermatogonium rs: round spermatid. Arabic numbers mark developmental steps of spermatids.

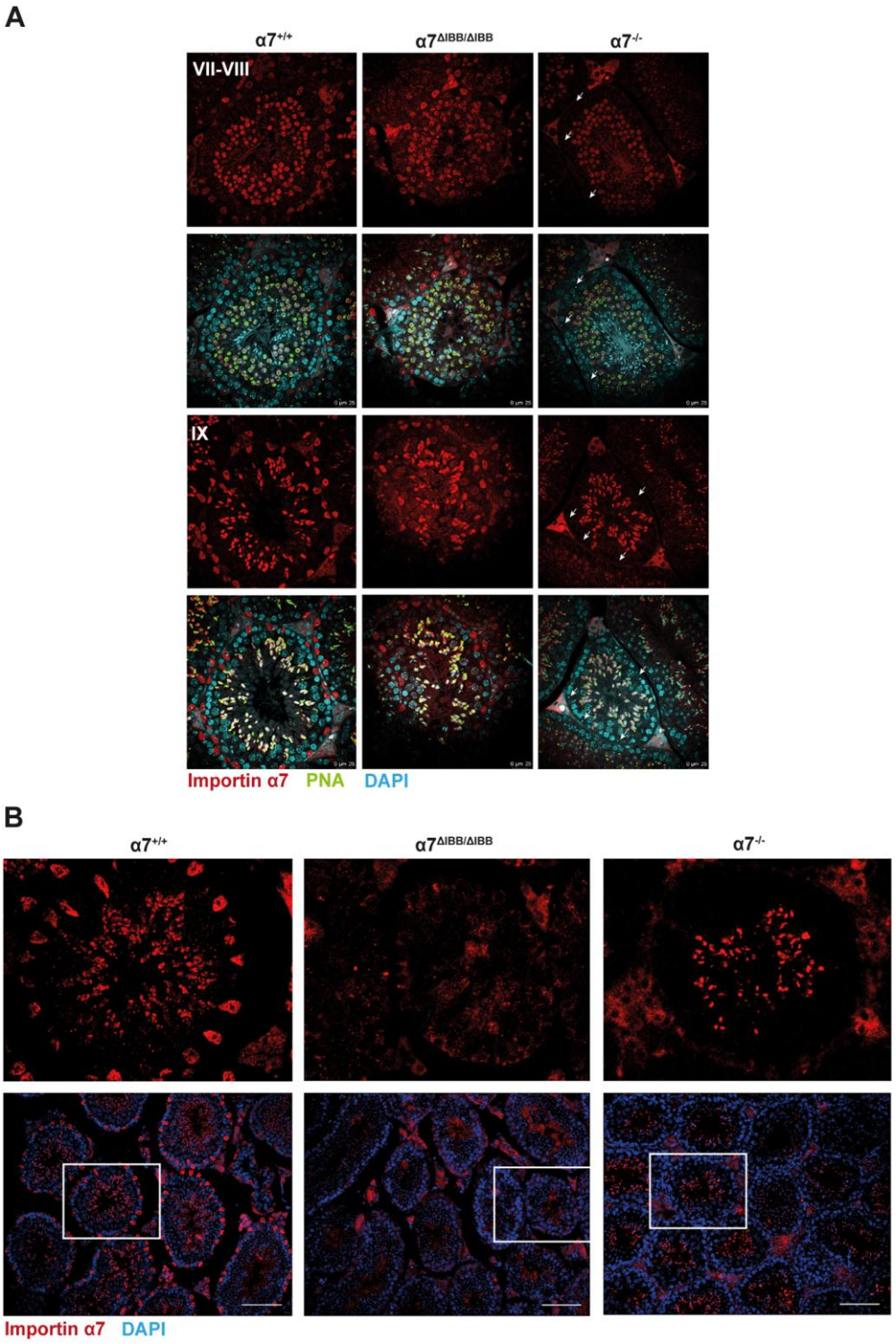

Fig. 4 Importin α7 is expressed in developing germ cells, but not in Sertoli cells of α7$^{-/-}$ mice. (A) Immunohistochemistry of testis using an antibody against the C-terminus of importin α7 (red); DAPI (blue); PNA (green). Note the absence of importin α7 in nuclei of Sertoli cells in α7$^{-/-}$ (arrows). Scale bars: 25 µm (B) Immunohistochemistry of testis sections using an antibody against the N-terminus of importin α7 (red); DAPI (blue). No specific

staining is observed in $\alpha7^{\Delta IBB/\Delta IBB}$ testis, as the antibody does not recognize the truncated protein. Importin α7 is expressed in round and elongating spermatids, but not in Sertoli cells of $\alpha7^{-/-}$ mice, while WT mice show a robust immunostaining in Sertoli cells (upper lane: inserts of lower lane). Age of mice: 12-16 weeks. Scale bars: 100 µm.

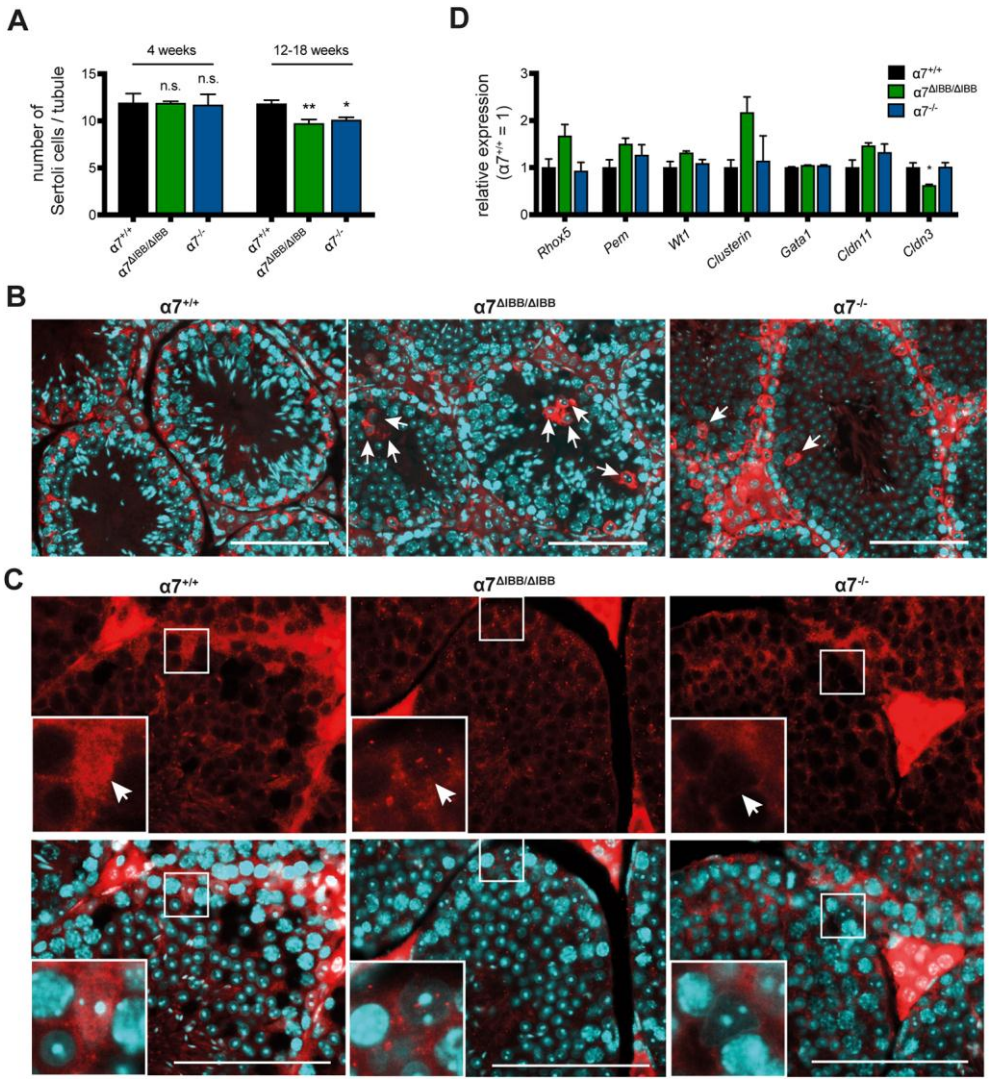

Fig. 5 Importin α7 deficiency decreases number of Sertoli cells and prevents nuclear import of AR. (A) Number of Sertoli cells per tubule. (B) Aberrant localization of Sertoli cell nuclei in seminiferous tubules of $\alpha7^{\Delta IBB/\Delta IBB}$ and $\alpha7^{-/-}$ testes (arrows). (C) Immunofluorescence of AR (red) in testis sections; DAPI (blue). Note the nuclear localization of AR in WT and the empty nuclei in $\alpha7^{\Delta IBB/\Delta IBB}$ and $\alpha7^{-/-}$ Sertoli cells (arrows). Scale bars: 100 µm. (D) Relative expression levels of selected genes in adult testes (12-20 weeks; n=6 per group).

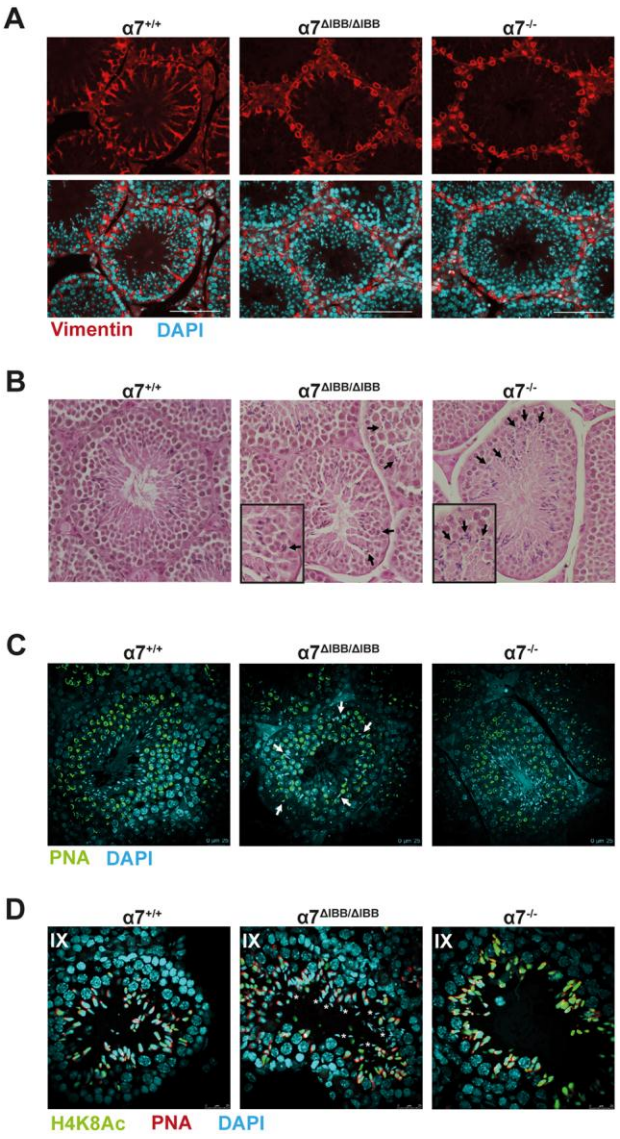

Fig. 6 Morphological and functional abnormalities in importin α7-deficient Sertoli cells. (A) Vimentin (red) and DAPI (blue) staining in testis paraffin sections; scale bars: 100 µm. (B) H&E staining of testis sections showing aberrant sperm orientation in seminiferous tubules of $\alpha7^{\Delta IBB/\Delta IBB}$ and $\alpha7^{-/-}$ testes. Arrows mark misoriented sperms. (C) DAPI (blue) and PNA (green) staining in testis sections showing defective sperm transport in $\alpha7^{\Delta IBB/\Delta IBB}$ testes. Arrows mark mislocalized sperms. (D) Sperm retention in stage IX seminiferous tubules. Sperm cells were labelled with against acetyl-Histone H4 (H4K8Ac, green), PNA (red) and DAPI (blue). Asterisks indicate sperm retention. Age: 12-16 weeks. Scale bars: 25 µm.

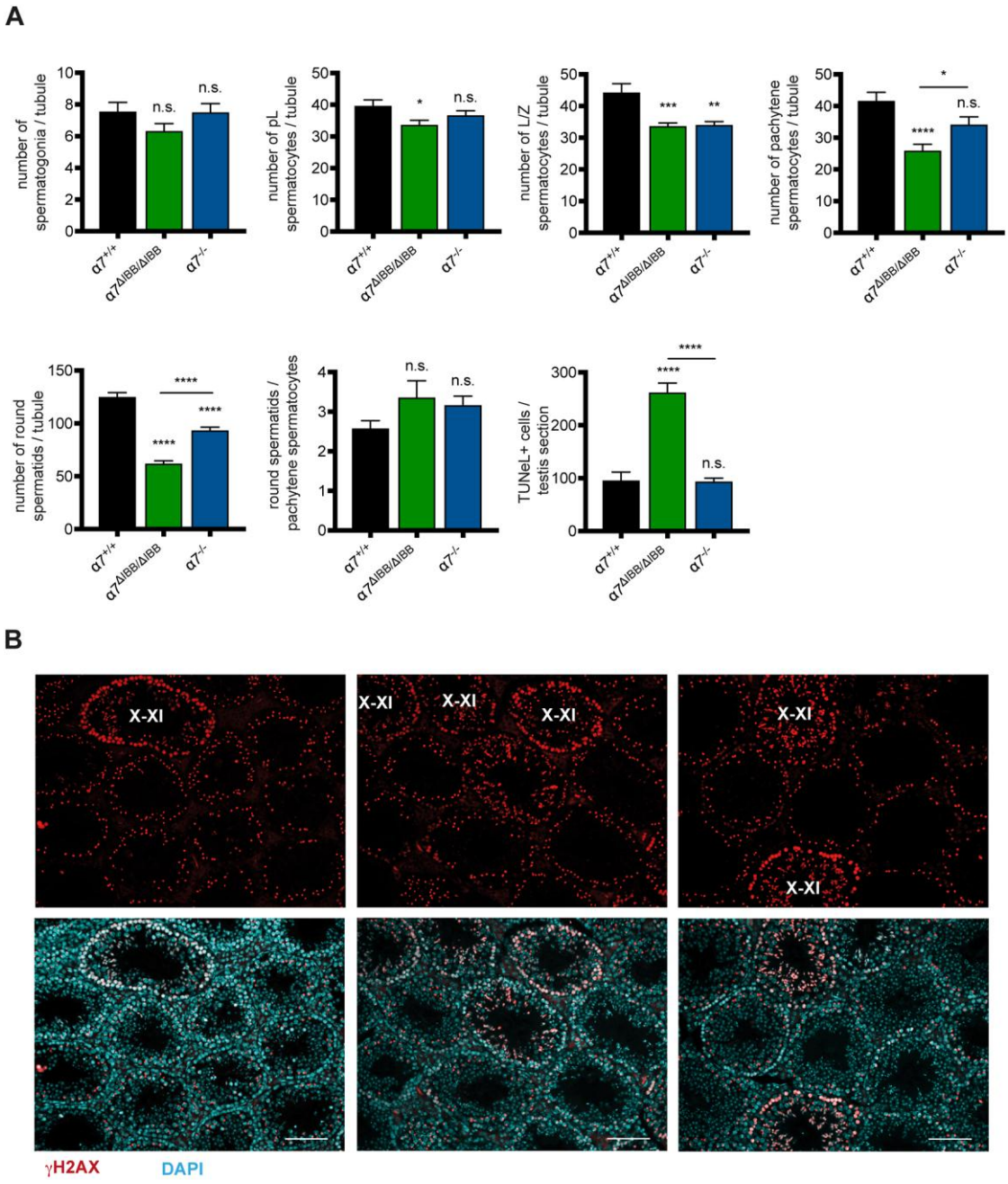

Fig. 7 Importin α7 deficiency results in loss of spermatocytes. (A) Number of germ cells at different developmental steps per seminiferous tubule in testes of mice aged 12-16 weeks; number of TUNEL-positive cells per testis section ($\alpha7^{+/+}$: n=6, $\alpha7^{\Delta IBB/\Delta IBB}$: n=7, $\alpha7^{-/-}$: n=8, 12-20 weeks); (B) γH2AX (red) and DAPI (blue) staining in adult testes. X-XI: stage X-XI tubules, scale bars: 100 µm.

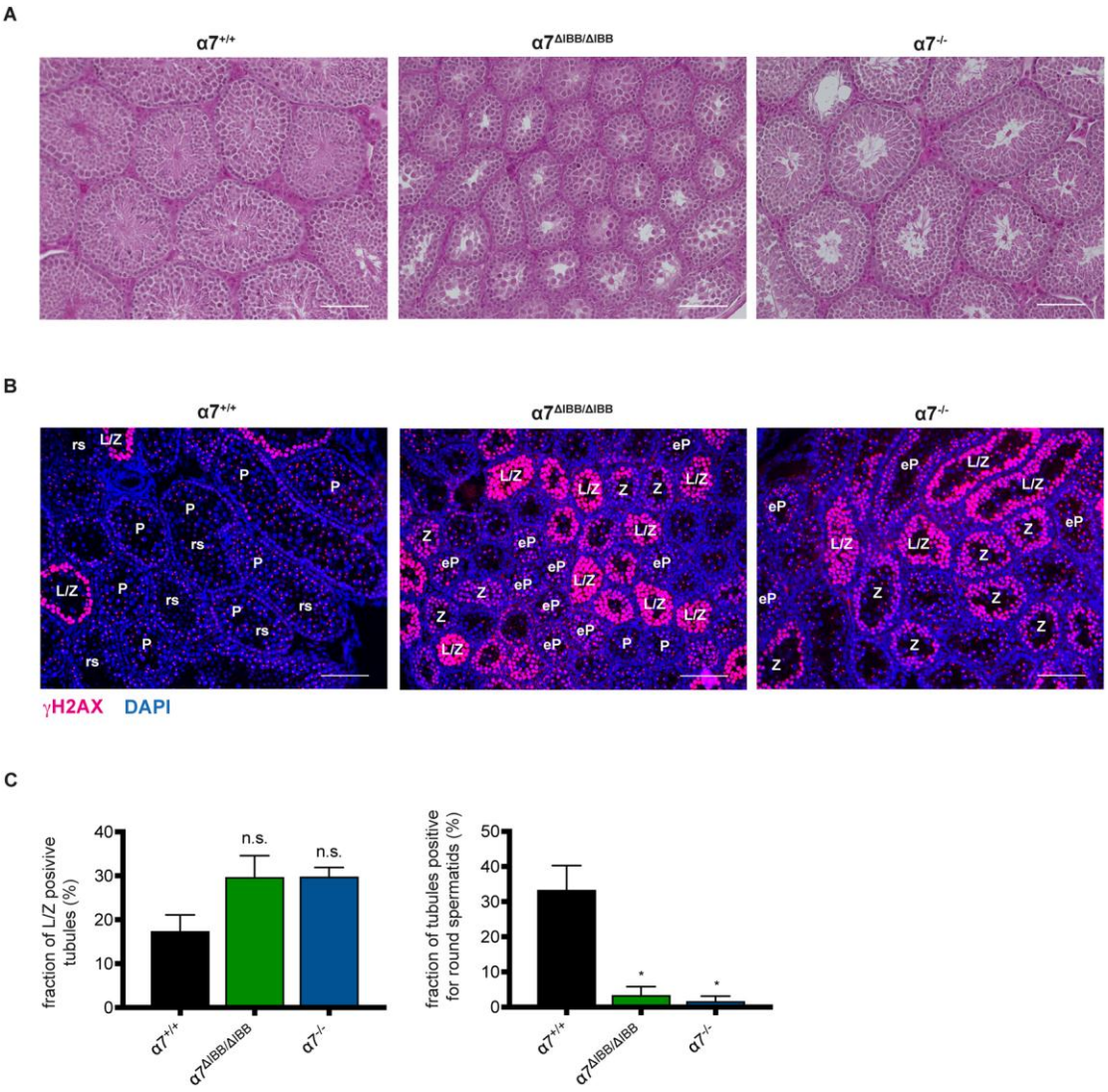

Fig. 8 Importin α7 deficiency causes a delay in the first spermatogenesis wave. (A) H&E staining of testis sections of WT, $\alpha7^{\Delta IBB/\Delta IBB}$ and $\alpha7^{-/-}$ mice at 6 weeks of age showing severely delayed onset of spermatogenesis. (B) γH2AX (red) and DAPI (blue) staining on testis sections of mice aged 21 days. L/Z: leptotene/zygotene spermatocytes; Z: zygotene spermatocytes, eP: early pachytene spermatocytes; P: pachytene spermatocytes; rs: round spermatids. Scale bars: 100 µm. (C) Quantification of tubules containing L/Z spermatocytes and round spermatids, respectively, per section in mice aged 21 days ($\alpha7^{+/+}$: n=5, $\alpha7^{\Delta IBB/\Delta IBB}$: n=5, $\alpha7^{-/-}$: n=3).

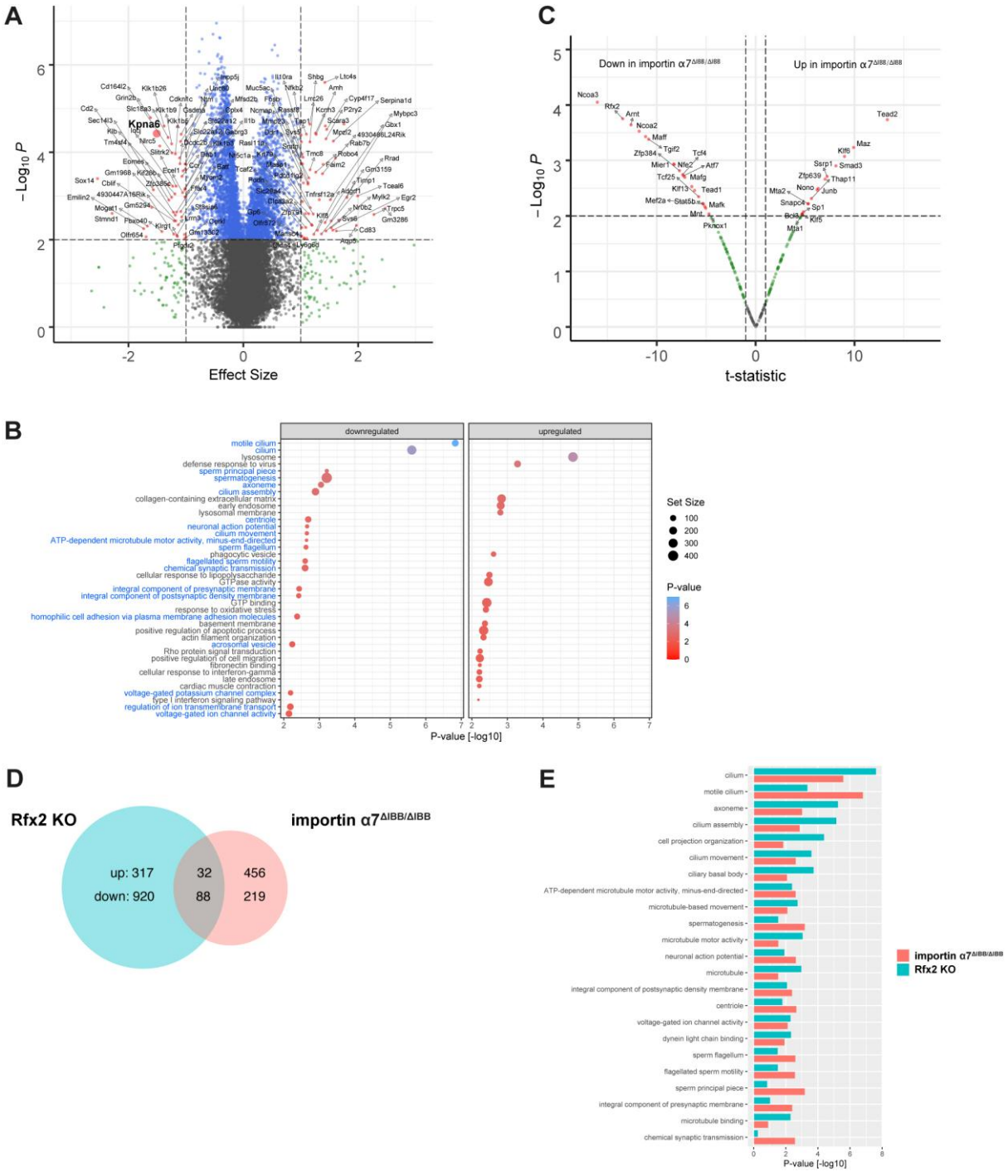

Fig. 9 Downregulated spermiogenesis-related pathways in importin α7-deficient testis. (A) Volcano plot depicting the differential gene regulation of the testes transcriptomes of WT and $\alpha7^{\Delta IBB/\Delta IBB}$ mice. The x- and the y-axes show the effect size according to a Wald test and the -$\log_{10}$ transformed p-value. Small red dots indicate significantly regulated genes according to p-value ($p<0.01$) and absolute effect size (>1). The *Kpna6* gene is indicated by an enlarged red circle. (B) Dotplot depicting the 20 most significantly up- and downregulated GO terms in the testes transcriptomes of $\alpha7^{\Delta IBB/\Delta IBB}$ mice compared to WT. The locus and color of the dots

indicate the -$\log_{10}$ p-value, while the dot size is related to the number of genes of the GO term. Blue and black row names refer to down- (blue) and upregulated (black) GO terms, respectively. (C) Volcano plot depicting the predicted differential TF activity of the testis transcriptomes of $\alpha7^{\Delta IBB/\Delta IBB}$ mice compared to WT. The x- and the y-axes show the t-statistic of a t-test and the -$\log_{10}$ transformed p-value. Red dots indicate significant differential TF activity according to the p-value ($p<0.01$) and the absolute t-statistic. (D) Venn diagramm showing the commonly and individually up- and downregulated genes from mouse testes in the Rfx2 KO and $\alpha7^{\Delta IBB/\Delta IBB}$ models in comparison to their respective WT controls (p-value cutoff<0.01, absolute effect size>0.5). (E) Barplot depicting the significance of 23 most downregulated GO terms in testes transcriptomes after importin α7 (red) or Rfx2 (GEO ID GSE68283, green) depletion according to a GSEA. The bars denote the -$\log_{10}$ transformed p-values.

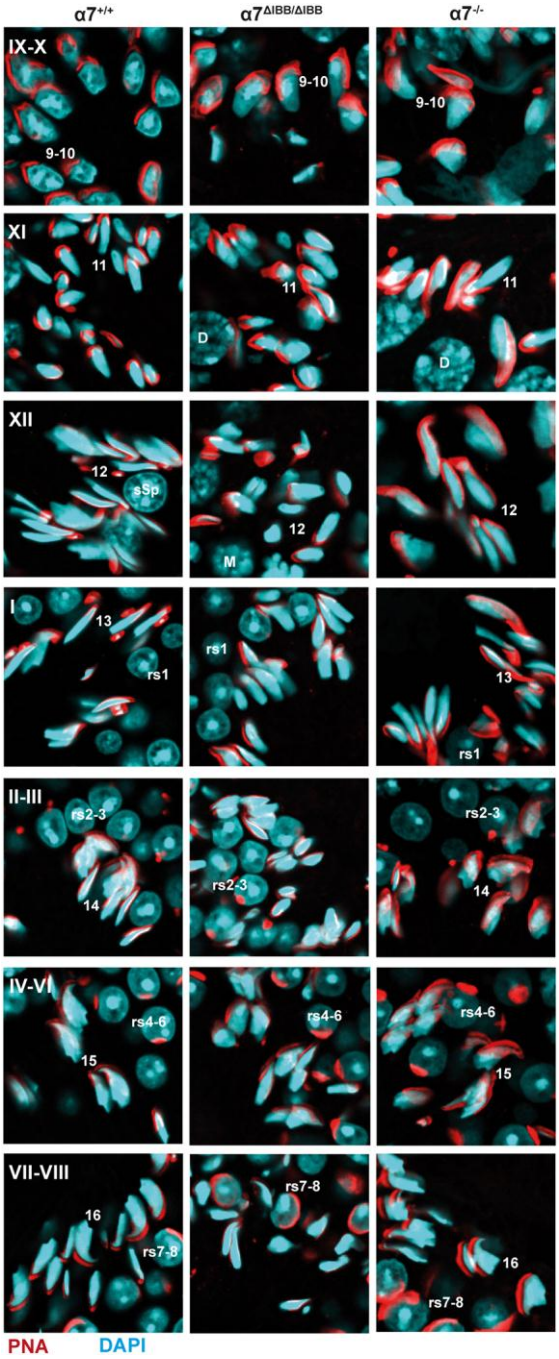

Fig. 10 Importin α7-deficient spermatids show abnormal elongation and nuclear shaping. Morphology of DAPI- (blue) and PNA-labelled (red) spermatids throughout their development. The deficiency/delay in elongation can be seen already in stage XII tubules. Roman numbers mark tubular stages, arabic numbers indicate the developmental step of spermatids. Note the abnormal configuration of sperm heads in $\alpha7^{\Delta IBB/\Delta IBB}$ spermatids. Age of mice: 12 weeks.

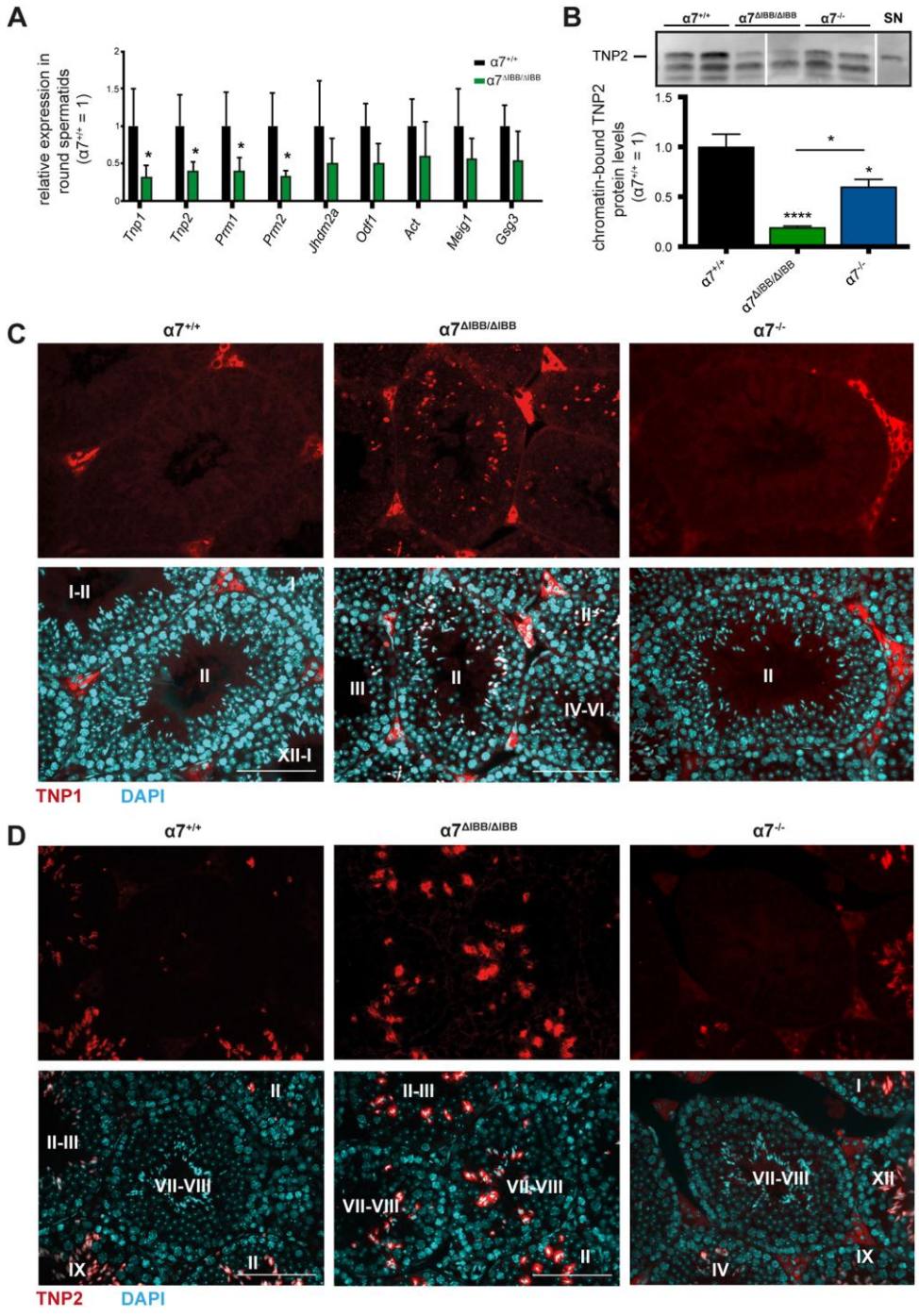

Fig. 11 Reduced expression of transition nuclear proteins and protamines in importin α7-deficient testes (A) Quantitative realtime PCR analysis of various postmeiotic genes in isolated round spermatids of adult (12-20 weeks) WT and $\alpha7^{\Delta IBB/\Delta IBB}$ testes ($\alpha7^{+/+}$: n=6, $\alpha7^{\Delta IBB/\Delta IBB}$: n=9). (B) Western blot analysis and quantification of TNP2 in WT $\alpha7^{\Delta IBB/\Delta IBB}$ and $\alpha7^{-/-}$ testis chromatin extracts. SN: not chromatin-associated TNP2 served as control. (C, D) TNP1 (C, red), TNP2 (D, red) and DAPI (blue) staining on sections of adult WT, $\alpha7^{\Delta IBB/\Delta IBB}$ and $\alpha7^{-/-}$ testes. Roman numbers mark the stage of seminiferous tubules; scale bars: 100 µm.

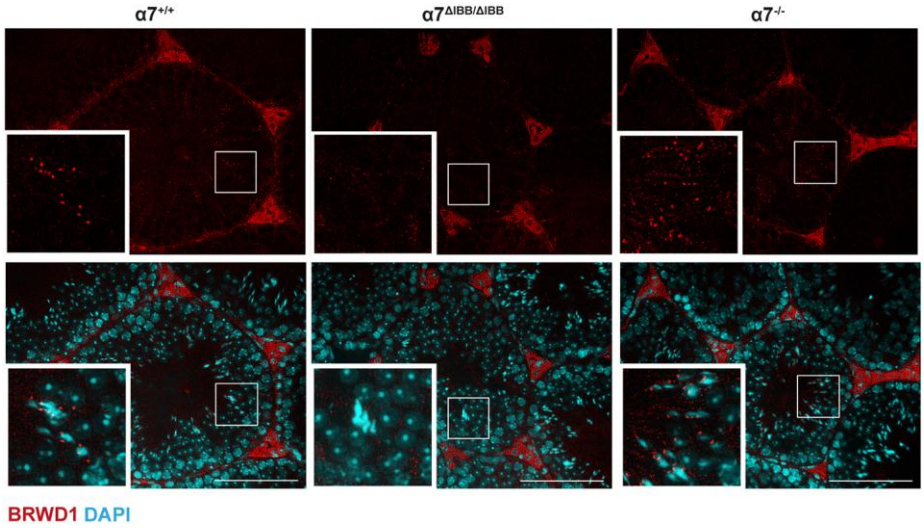

Fig. 12 Disturbed localization of BRWD1 in importin α7$^{-/-}$ testes Immunofluorescence for BRWD1 (red) in WT, α7$^{\Delta IBB/\Delta IBB}$ and α7$^{-/-}$ testis on paraffin sections; counterstained with DAPI (blue), scale bars: 100 µm. Age of mice: 12-16 weeks.

Fig. S1

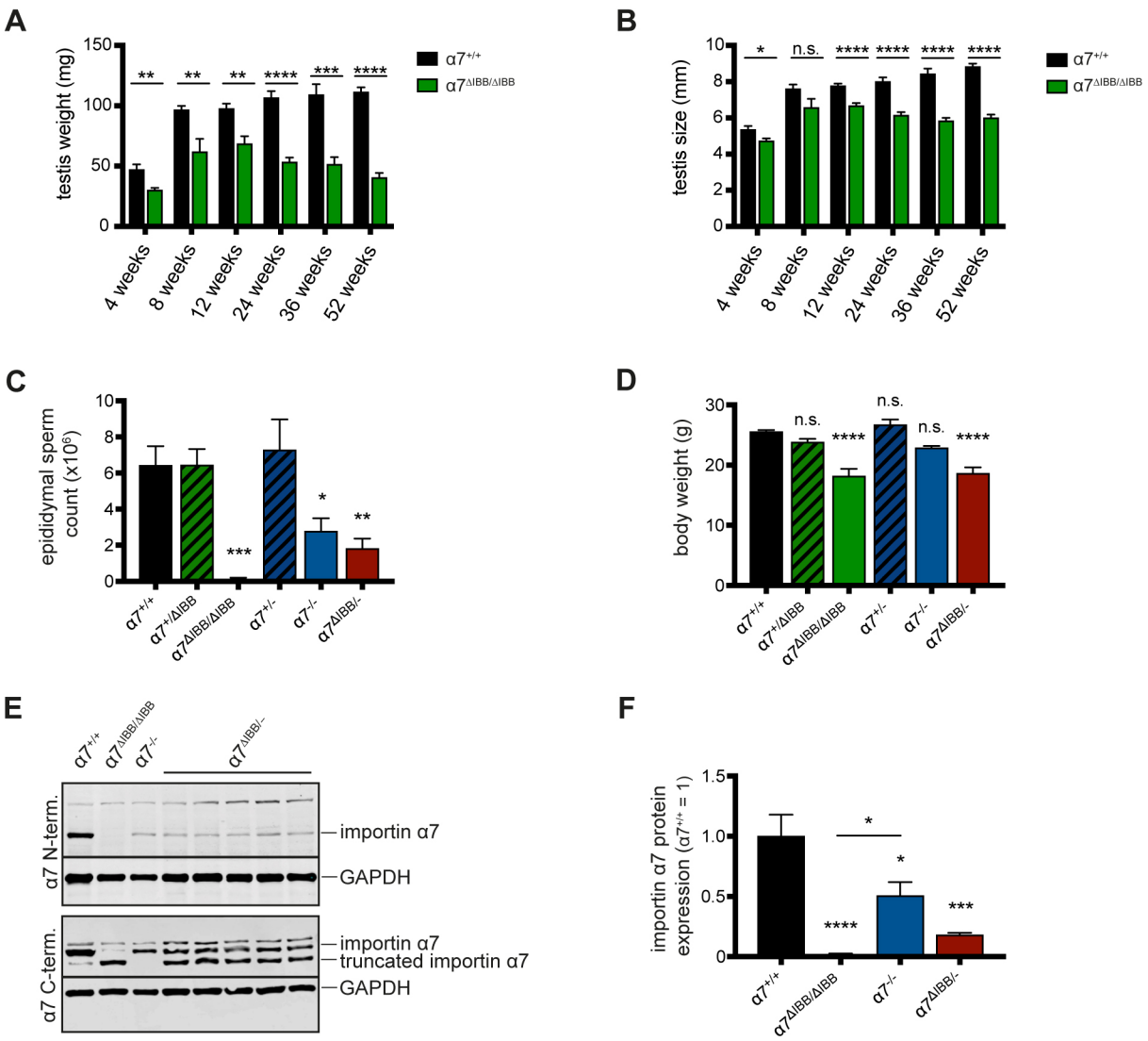

Fig. S1. (A) Testis weight at various time points (n=6-18). (B) Testis size at various time points (n=6-18). (C) Epididymal sperm count of all mutant lines (aged 9 weeks) including compound heterozygous mice ($\alpha7^{\Delta IBB/-}$) compared to WT mice (n=4-6). (D) Body weight of all mutant mouse lines (aged 9 weeks). (E) Western blot analysis of testis protein extracts with anti-importin α7 antibodies show, that $\alpha7^{\Delta IBB/-}$ testes express the full-length and the truncated protein. Part of this Western blot is shown in Fig. 1B. (F) Quantification of Western blots using the N-terminal antibody reveals a further reduction in expression of importin α7 in $\alpha7^{\Delta IBB/-}$ testes (n=4-5).

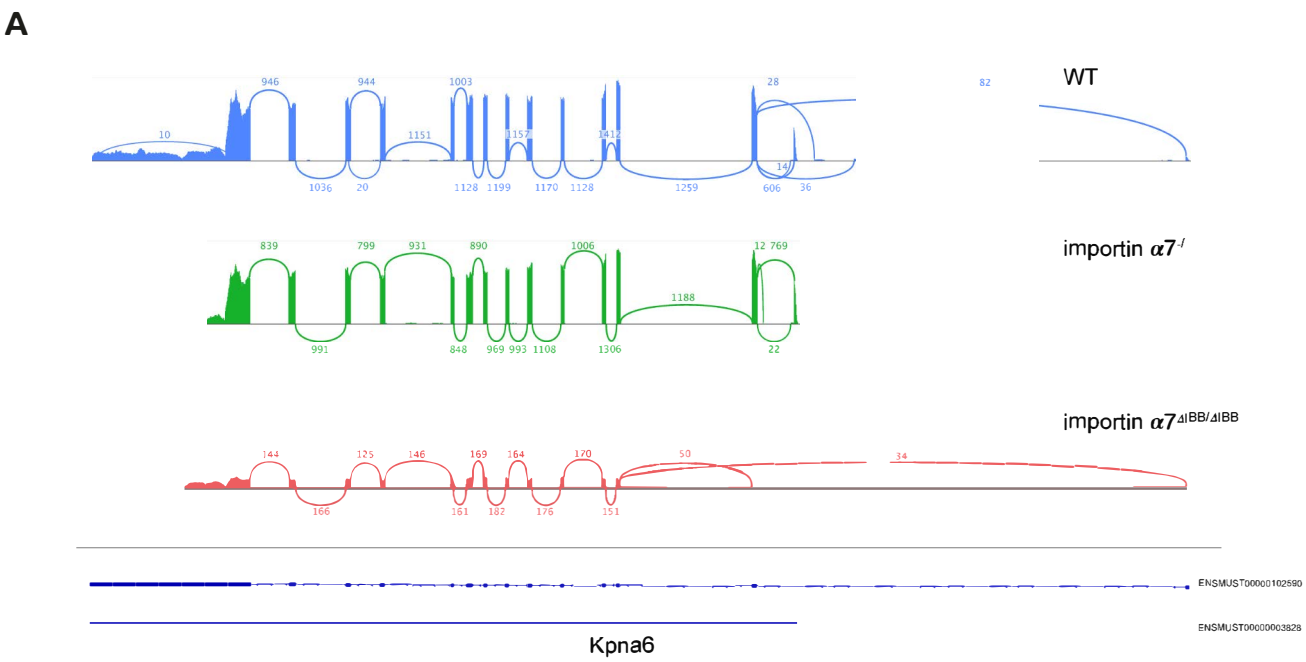

Fig. S2. (A) The Sashmi plot depicts a histogram of the number of reads covering the exons on Chr4 of the murine *Kpna6* genes in WT (top) and under the two knockout conditions ($\alpha7^{-/-}$ and $\alpha7^{dIBB/dIBB}$, middle and bottom). The numbers above or below the connecting arcs denote the number of reads spanning across the respective exons. The two *Kpna6* transcripts are depicted below in dark blue showing the exon/intron structure. Black numbers above the transcripts mark the position on the chromosome. Note how in the $\alpha7^{-/-}$ condition the first exon is missing (corresponding to the longer transcript; Ensembl database ENSMUST00000102590), while the shorter transcript (ENSMUST00000003828; starting from exon1A) is fully expressed. Contrary to this, $\alpha7^{dIBB/dIBB}$ shows an approximately five-fold reduced number of reads across all exons. Here, no expression from exon1A is detected (which is deleted), and a low number of reads is detected from exon2, which is only partly deleted by conventional knockout technology. (B) RT-PCR of importin α7 transcripts in FACS-sorted round spermatids. In WT germ cells, both promoters are used, while in $\alpha7^{-/-}$ germ cells, only transcription from the intronic promoter can be found. M: 100bp marker.

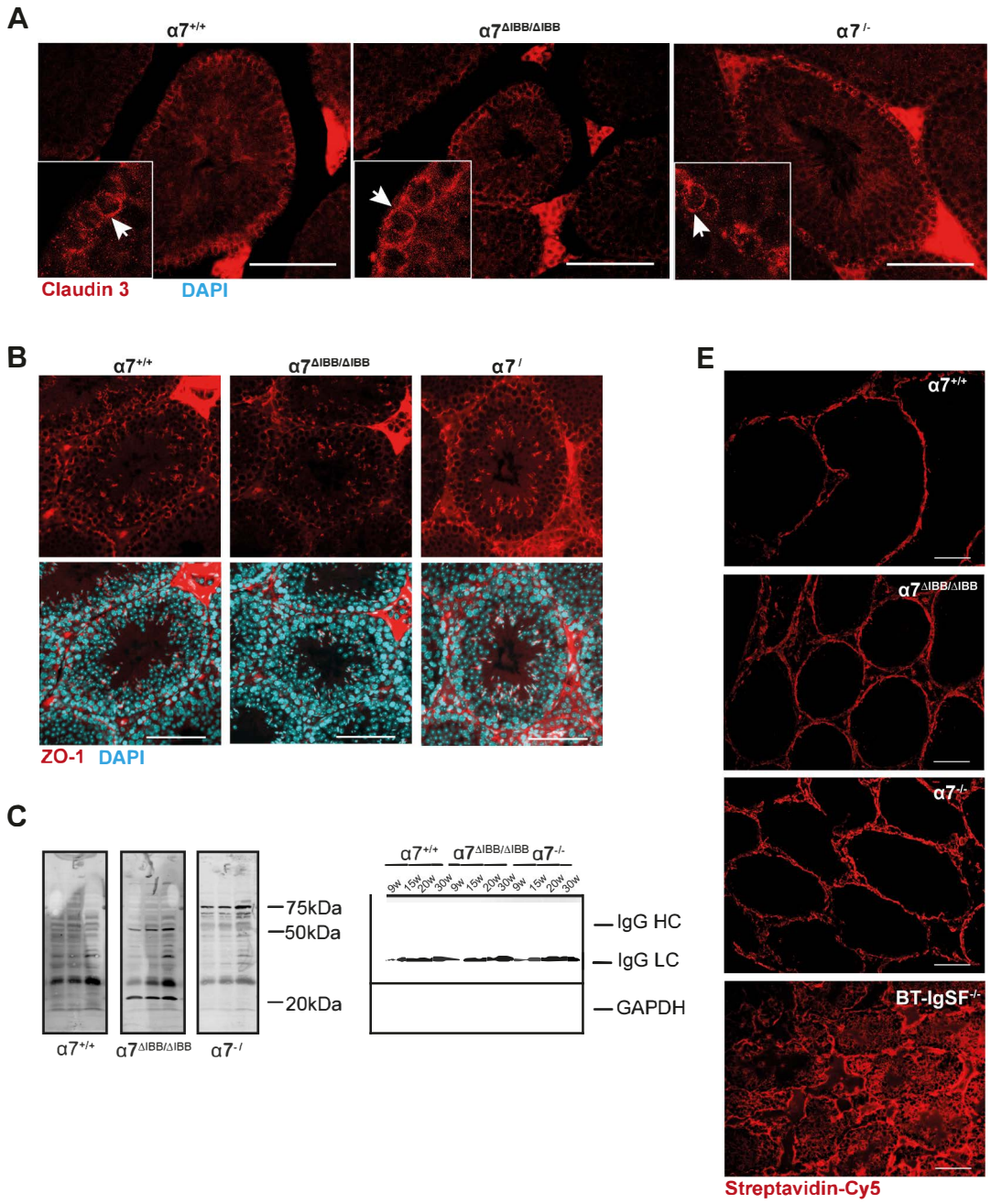

Fig. S3. (A) Cldn3 (red) and DAPI (blue) staining of adult WT, $\alpha7^{\Delta IBB/\Delta IBB}$ and $\alpha7^{-/-}$ testes. Arrows mark Cldn3 staining of stage VIII seminiferous tubules. Scale bars: 100 µm. (B) ZO-1 (red) and DAPI (blue) staining of testis sections of WT, $\alpha7^{\Delta IBB/\Delta IBB}$ and $\alpha7^{-/-}$ mice. Scale bars: 100 µm. (C) Western blot analysis of WT testis protein extracts probed with sera from WT, $\alpha7^{\Delta IBB/\Delta IBB}$ and $\alpha7^{-/-}$ mice at 16 weeks of age. Lines mark 20-, 50- and 75-kDa testicular antigens recognized by antibodies (autoantibodies) present in serum samples of different $\alpha7^{\Delta IBB/\Delta IBB}$ and $\alpha7^{-/-}$ but not WT males. (D) Representative Western blot of immunoglobulins in testis extracts of WT, $\alpha7^{\Delta IBB/\Delta IBB}$ and $\alpha7^{-/-}$ mice at different ages. (E) Biotin diffusion assay marking the integrity of the BTB. Biotin is visualized by streptavidin-Cy5 staining (red). The $\alpha7^{\Delta IBB/\Delta IBB}$ and $\alpha7^{-/-}$ tubules show no major changes of biotin distribution compared to WT seminiferous tubules. As a control, a BT-IgSF knockout mouse was analyzed, which has recently been published to show a severe disruption of the BTB (Pelz et al., 2017). Scale bars: 100 µm.

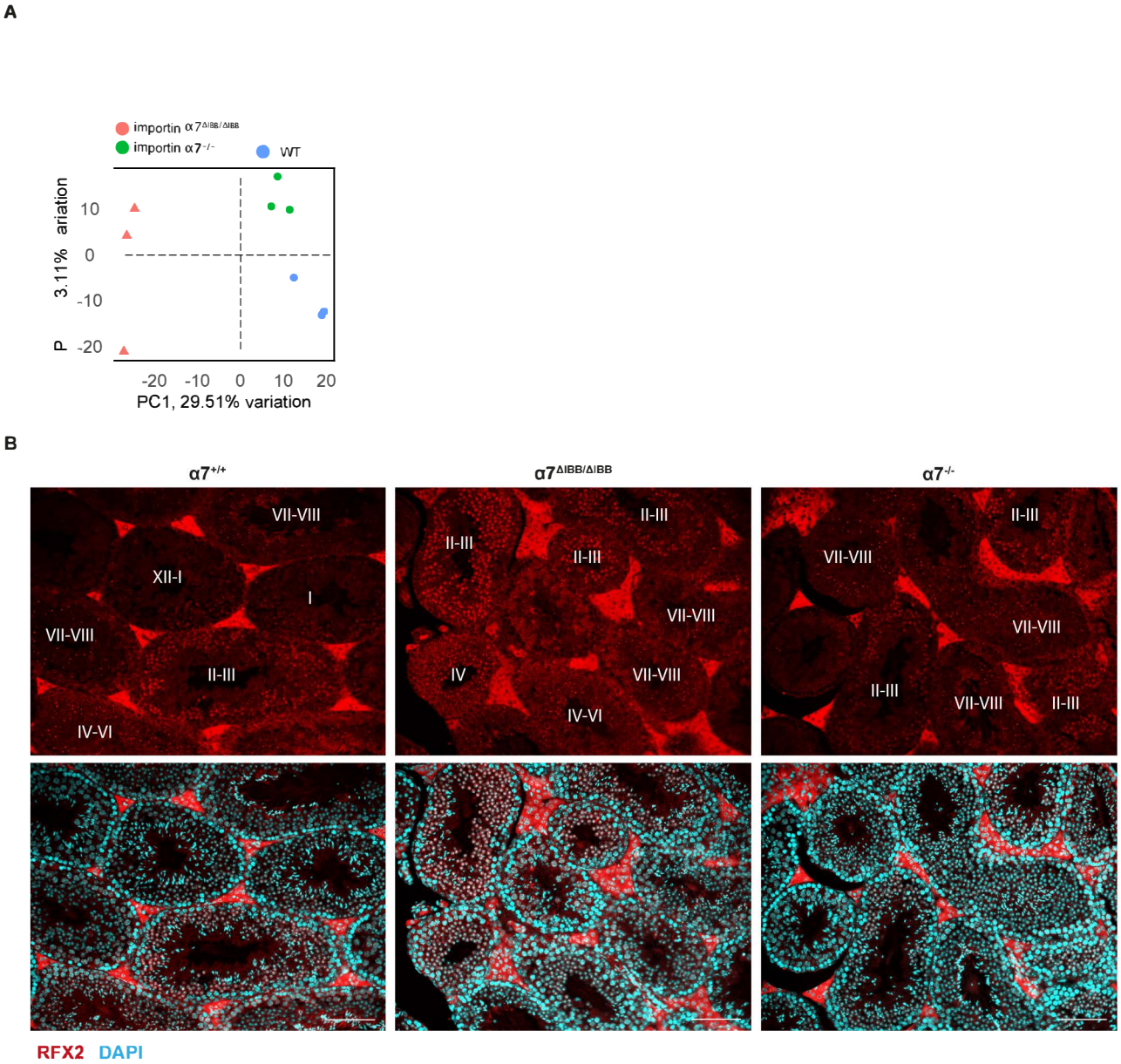

Fig. S4. (A) Principal component analysis of the gene-aggregated expression values as measured in transcripts per million of the 50% most variable genes across all samples. (B) Immunofluorescence for Rfx2 in WT, $\alpha7^{\Delta IBB/\Delta IBB}$ and $\alpha7^{-/-}$ testis on paraffin sections. Rfx2 is strongly expressed in nuclei of step 2-3 round spermatids. In step 4-8 round spermatids the protein localizes to a distinct spot in the nucleus, and when elongation of spermatids starts, the protein cannot be detected anymore. No abnormal staining pattern could be observed in importin $\alpha7^{dIBB/dIBB}$ or $\alpha7^{-/-}$ testes. Roman numbers mark the tubular stages. Scale bars: 100 µm.

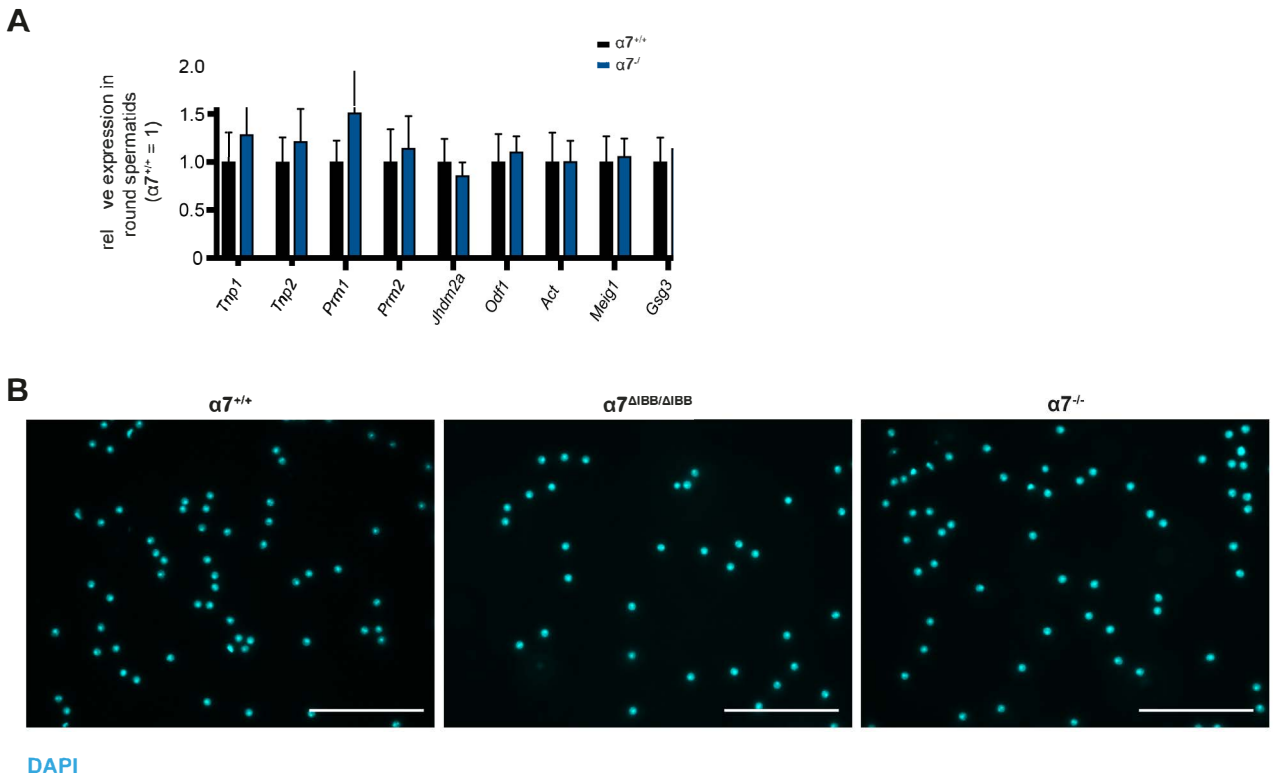

Fig. S5. (A) Quantitative realtime PCR analysis of various postmeiotic genes in isolated round spermatids of adult (12-20 weeks of age) WT and $\alpha7^{-/-}$ testes (n=4-6). (B) Following FACS-sorting, every sample was assessed with regard to purity of sorted round spermatids (average ± SD: WT 95.4% ± 0.02, $\alpha7^{\Delta IBB/\Delta IBB}$ 93.2% ± 0.03, $\alpha7^{-/-}$ 90.9% ± 0.03, no cells other than round spermatids or elongating sperms were found in the FACS-sorted samples). Scale bars: 100 µm.

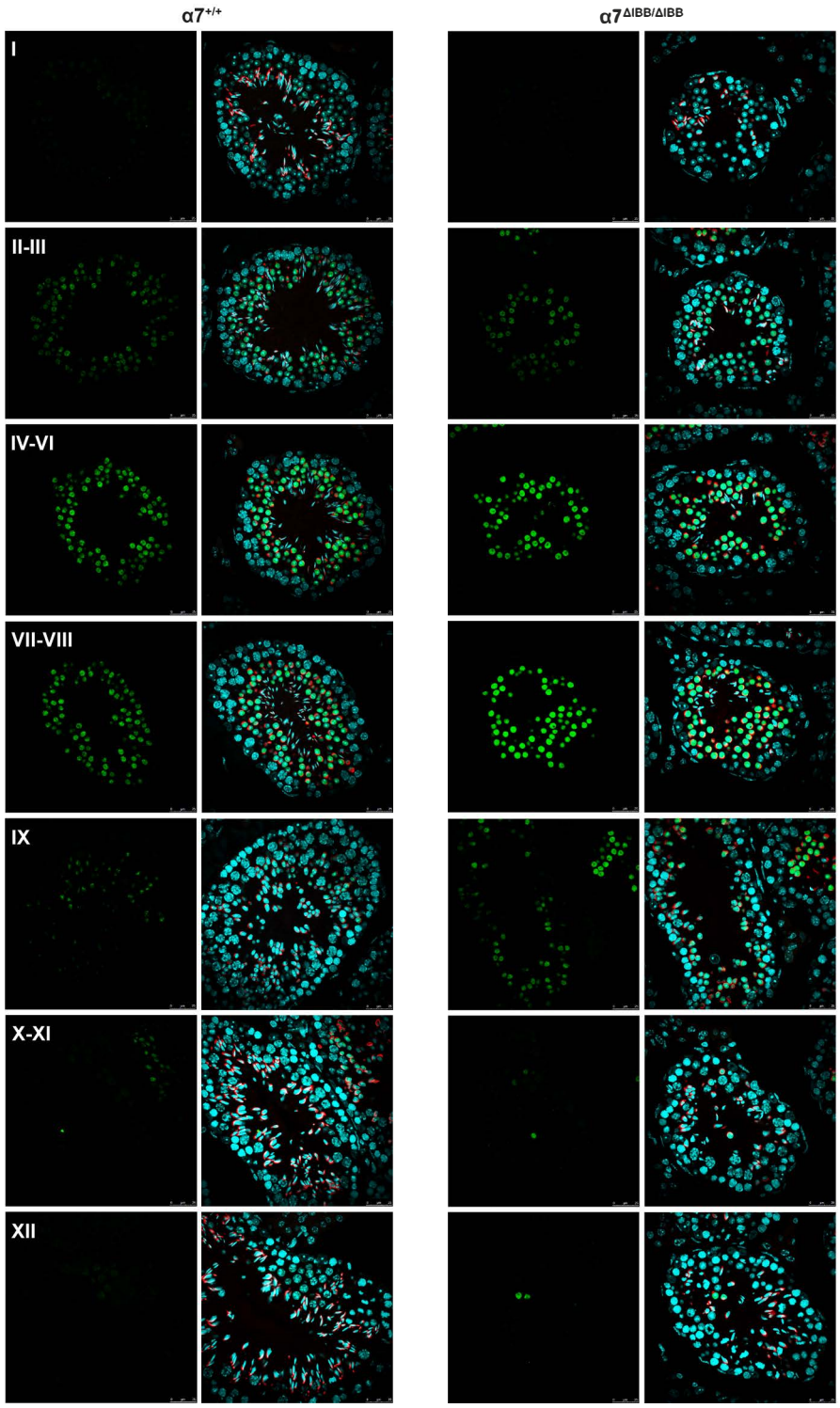

Fig. S6. Immunofluorescence for Crem (green) in WT and $\alpha7^{\Delta IBB/\Delta IBB}$ testis, counterstained with DAPI (blue) and PNA (red, merge right panel). Scale bars: 25 µm.

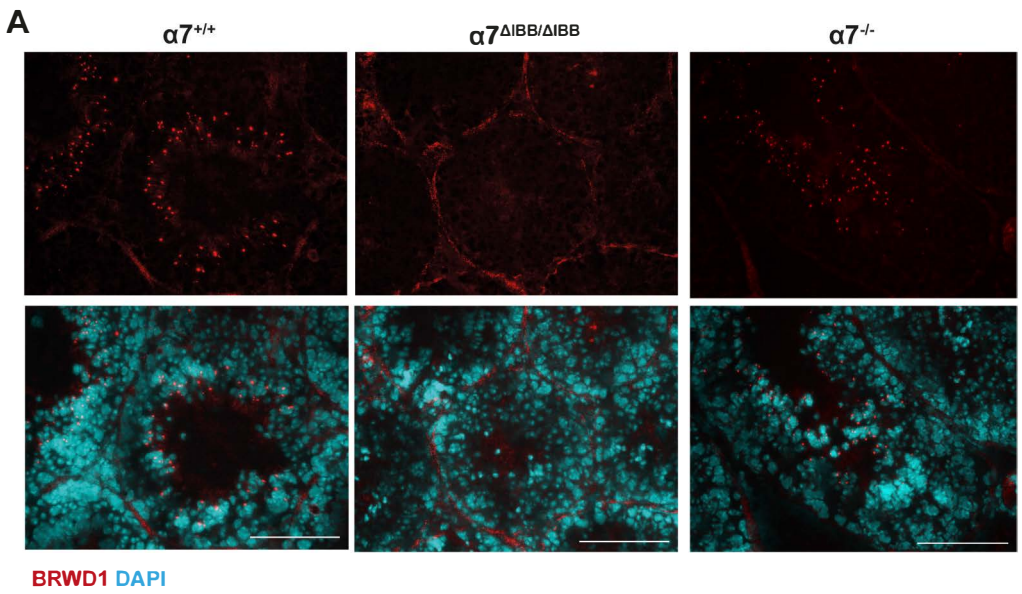

Lorem ipsum

Fig. S7. (A) Immunofluorescence for BRWD1 (red) in WT, $\alpha7^{\Delta IBB/\Delta IBB}$ and $\alpha7^{-/-}$ testis on snap-frozen cryosections; counterstained with DAPI (blue), scale bars: 100 µm. (B) Quantification of BRWD1 Western blot signals normalized to ß-tubulin ($\alpha7^{+/+}$: n=4, $\alpha7^{\Delta IBB/\Delta IBB}$: n=4, $\alpha7^{-/-}$: n=6). Age of mice: 12-16 weeks.

Table S1. List of genes, which are differentially expressed in $\alpha7^{\Delta IBB/\Delta IBB}$ and $\alpha7^{-/-}$ testes compared to WT and to each other. Significantly regulated genes (p-value < 0.01; absolute effect size > 1) are highlighted.

Click here to download Table S1

Table S2. List of genes, which are differentially expressed in testis of Rfx2 KO or in $\alpha7^{\Delta IBB/\Delta IBB}$ compared to their respective WT controls (P-value cutoff < 0.01, absolute effect size > 0.5).

Click here to download Table S2

Table S3. GSEA of $\alpha7^{\Delta IBB/\Delta IBB}$ and Rfx2 knockout testes.

Click here to download Table S3

Table S4. List of primary and secondary antibodies

Name	Company	Conditions
Importin α7 (C-terminal)	selfmade (peptide QPEAPMEGFQL) (Kohler et al. 1999)	1:10,000 (Western blot) 1:1,000 (Immunofluorescence)
Importin α7 (N-terminal)	selfmade (peptide MASPGKDNYR) (Kohler et al. 1999)	1:2,000 (Western blot) 1:200 (Immunofluorescence)
WT1	Abcam (#15249)	1:100 (Immunofluorescence)
Androgen receptor	Santa Cruz Biotechnology (10310, #sc816G)	1: 1000 (Western blot) 1:100 (Immunofluorescence)
Claudin 3	Acris Antibodies (# AP15488PU)	1:100 (Immunofluorescence)
ZO-1	Invitrogen (#339100)	1:100 (Immunofluorescence)
Vimentin	Cell signalling (#5741)	1:100 (Immunofluorescence)
ß3 Tubulin	Abcam (#ab52901)	1:100 (Immunofluorescence)
acetyl-Histone H4 (Lys8)	Upstate (#06-760)	1:200 (Immunofluorescence)
SALL4	Santa Cruz Biotechnology (EE-30, #sc101147)	1:100 (Immunofluorescence)
anti-BrdU	Biozol (#OBT0030)	1:500 (Immunofluorescence)
γH2Ax (Ser 139)	Cell Signaling (#9718)	1:200 (Immunofluorescence)
TNP1	Invitrogen (#PA5-44078)	1:200 (Immunofluorescence)
TNP2	Santa Cruz Biotechnology (K18, #sc21106)	1:1,000 (Western blot) 1:100 (Immunofluorescence)
ß-Actin	Cell Signaling (#4967)	1:1,000 (Western blot)
GAPDH	Cell Signaling (#2118)	1:1,000 (Western blot)
dimethyl-Histone H3 (Lys9)	Upstate (#07-441)	1:100 (Immunofluorescence)
trimethyl-Histone H3 (Lys9)	Millipore (#05-1242)	1:100 (Immunofluorescence)
acetyl-Histone H3 (Lys9)	Sigma-Aldrich (#06-942)	1:100 (Immunofluorescence)
acetyl-Histone H3 (Lys14)	Millipore (#06-911)	1:100 (Immunofluorescence)
acetyl-Histone H4 (Lys12)	Upstate (#07-595)	1:100 (Immunofluorescence)
RFX2	Novus (#NBP2-13224)	1:100 (Immunofluorescence)
CREM	Novus (#NBP1-81760)	1:500 (Immunofluorescence)
BRWD1	Biorbyt (#orb255836)	1:100 (Immunofluorescence)
Lectin-PNA Alexa 488	life technologies (#L21409)	1:500 (Immunofluorescence)
Lectin-PNA Alexa 594	life technologies (#L32459)	1:500 (Immunofluorescence)
IRDye 800 donkey anti-mouse	LiCor (#926-32212)	1:10,000 (Western blot)
IRDye 800 donkey anti-rabbit	LiCor (#926-32213)	1:10,000 (Western blot)
streptavidin-Cy5	Thermo Fisher Scientific (#434316)	1:600 (Immunofluorescence)
goat anti-mouse Cy3	Abcam (#ab97035)	1:500 (Immunofluorescence)
goat anti-mouse Alexa 488	Invitrogen (#A110019)	1:500 (Immunofluorescence)
donkey anti-rabbit Cy3	Jackson ImmunoResearch (#711-165-152)	1:500 (Immunofluorescence)
donkey anti-rabbit Alexa 488	Invitrogen (#A21206)	1:500 (Immunofluorescence)
donkey anti-rat Cy3	Jackson ImmunoResearch (#711-165-153)	1:500 (Immunofluorescence)

Table S5. List of primers of target genes for PCR and real-time PCR

gene	Forward sequence (5'->3')	Reverse sequence (5'->3')
Kpna6	Ex1: AGG CTA CCG CTG AAG CTA CC Ex1A: GGG ACA GCA CAG GCT CAA TC Ex2: GCC TTA AAC CCT GAG GAA ATG	Ex6: GAC GTT CCA GAG GCA ATG TT
Rhox5	CAAGGAAGACTCGGAAGAACAG	CATAGGACCAGGAGCACCAG
Pem	CAAAATCTCGGTGTCGCAAA	GCAACACCAGTCCCTGAACA
Wt1	CCG CAA CCA AGG ATA CAG CAC	GGG GTC CTC GTG TTT GAA GG
Clusterin	GGTCCGCAGCCTCATGTC	CATCTCAAAGAAAGGCTGGAACA
Gata1	CAT CAG CAC TGG CCT ACT AC	GTA GAG TGC CGT CTT GCC ATA G
Cldn11	CGT CAT GGC CAC TGG TCT CT	GGC TCT ACA AGC CTG CAC GTA
Cldn3	GCGCCTTGCTGTGTTGCT	AGAGGATCTTGGTGGGTGCAT
Tnp1	GAGAGGTGGAAGCAAGAGAAAA	CCCACTCTGATAGGATCTTTGG
Tnp2	CTGCCCCAAGAACAGGAAGA	CCGTTTCCGCCTCCTGA
Prm1	AGGTGTAAAAAATACTAGATGCACAGAAT AG	TTCAAGATGTGGCGAGATGCT
Prm2	GAATAGTCACCTGCCCAAGCA	GCAGCTCAGGGCTCAGACA
Jhdm2a	TGAAGGAAAAGAGAAGCCAGG	CTGATCGTGGATAGGGTCATG
Odf1	CCATCGCTCCGCAGTTTAG	AGACCTTCCCATCTTTCACG
Act	ACAGACTGCTATTCCAACGAG	TTGGTTCCTATTGGCTGTCG
Meig1	AACAAGCAGGATATCGGGATG	AAAGTATTGTCCCTCCGCTG
Gsg3	TGAGTAACACCTTGAATGGGC	CTCTTTCCTACTCAAGACGCTG
Gapdh	CTTTGTCAAGCTCATTTCCTGG	TCTTGCTCAGTGTCCTTGC